PB-248 590

THE FORMATION OF AEROSOLS IN A PHOTOCHEMICAL FAST FLOW REACTOR

M. Lipeles, et al

Rockwell International Corporation

Prepared for:

Environmental Protection Agency

July 1975

DISTRIBUTED BY:

NTIS

National Technical Information Service
U. S. DEPARTMENT OF COMMERCE

PB 248 590

Reproduced by
NATIONAL TECHNICAL
INFORMATION SERVICE
US Department of Commerce
Springfield, VA. 22151

016040

SC551.17FR

THE FORMATION OF AEROSOLS IN A PHOTOCHEMICAL FAST FLOW REACTOR

FINAL REPORT

JULY 1975

GENERAL ORDER NO. 551

CONTRACT NO. 68-02-0771/CAPA-8-71(1-73)

Prepared for

Environmental Protection Agency
Research Triangle Park, NC 27711

and

Coordinating Research Council
New York, NY 10020

by

M. Lipeles
Principal Investigator

with

D. A. Landis and G. M. Hidy

Reproduced by
NATIONAL TECHNICAL
INFORMATION SERVICE
US Department of Commerce
Springfield, VA. 22151

Science Center
Rockwell International

1049 CAMINO DOS RIOS
THOUSAND OAKS, CALIF. 91360

805/498-4545

BIBLIOGRAPHIC DATA SHEET	1. Report No. CRC-APRAC-CAPA-8-71-4	2.	3. Recipient's Accession No.

4. Title and Subtitle
The Formation of Aerosols in a Photochemical Fast Flow Reactor

5. Report Date
July 1975

6.

7. Author(s)
M. Lipeles; D. A. Landis; G. M. Hidy

8. Performing Organization Rept. No. SC551.17FR

9. Performing Organization Name and Address
Rockwell International
1049 Camino Dos Rios
Thousand Oaks, California 91360

10. Project/Task/Work Unit No.

11. Contract/Grant No.

12. Sponsoring Organization Name and Address
Environmental Protection Agency, Research Triangle Park, North Carolina 27711 and Coordinating Research Council, Inc., 30 Rockefeller Plaza, New York, N. Y. 10020

13. Type of Report & Period Covered
Final

14.

15. Supplementary Notes
Not releasable to the public until January 1976.

16. Abstracts
This report details work performed on the study of aerosol formation in a photochemical fast flow reactor which may be operated in a "wall free" mode. Aerosols have been produced in this reactor in irradiated dry air containing typically 0.8 ppm NO_2 and 10 ppm of one hydrocarbon. The hydrocarbons studied were α-pinene, 1-hexene, cyclohexene, 1-dodecene, toluene, m-xylene, 1,3-hexadiene, and 1,5 hexadiene. The effect of the addition of various mixtures of SO_2, H_2O and NH_3 to the reactions was studied. Ozone and condensation nuclei concentration were measured in the reactor as a function of reactant concentration. Total mass production was measured by filter collection, and infrared spectra of some of the samples have been obtained.

17. Key Words and Document Analysis. 17a. Descriptors

Air Pollution
Ozone
-Pinene
Cyclohexene
M-Xylene
Hexadiene
Dodecene
Nitrogen Dioxide
Sulfur Dioxide
Photochemical
Hydrocarbons

17b. Identifiers/Open-Ended Terms

17c. COSATI Field/Group 07B; 07C; 07E;13B

18. Availability Statement
Releasable to the general public.

19. Security Class (This Report) UNCLASSIFIED

20. Security Class (This Page) UNCLASSIFIED

21. No. of Pages 75

22. Price 4.50

FORM NTIS-35 (REV. 3-72)
THIS FORM MAY BE REPRODUCED
USCOMM-DC 14952-P72

TABLE OF CONTENTS

		Page
List of Figures		iii
List of Tables		iv
Abstract		1
1.	Introduction	2
2.	Experimental Program with the Prototype Reactor	6
	2.1 Ozone Measurements	6
	2.2 Actinometry	8
	2.3 Flow Visualization	9
	2.4 Aerosol Experiments with the Prototype Reactor	9
	2.5 Conclusions on the Prototype Reactor	11
3.	The New Reactor System	12
	3.1 The New Reactor	12
	3.1.1 Flow Theory for the New Reactor	12
	3.1.2 The New Reactor Design	13
	3.1.3 Flow Visualization in the New Reactor	15
	3.1.4 Advantages of the New Reactor	16
	3.2 Modifications in the Gas Handling System	16
4.	Experimental Procedures	17
	4.1 Ozone & Condensation Nuclei Measurements	17
	4.2 Filter Collections	18
	4.3 Infrared Analysis	18
5.	Results	19
	5.1 Condensation Nuclei and Ozone Data	19
	5.2 Filter Collections	44
	5.3 Chemical Analysis	44
6.	Discussion	50
	6.1 Hydrocarbon Effect on Ozone Production	50
	6.2 Nuclei Production	52
	6.3 Speculations About Mechanism	55

TABLE OF CONTENTS (continued)

	Page
6.4 Atmospheric Aerosol Processes	57
Appendix A	61
Appendix B	65
References	67

LIST OF FIGURES

		Page
Figure 1.	Ozone Measurements with the Dilution Probe in the Prototype Reactor	7
Figure 2.	Smoke Visualization of Flow in Prototype Reactor	10
Figure 3.	Scale Diagram of the New Reactor	14
Figure 4.	The Effect of Initial NO_2 Concentration on Ozone Production with α-Pinene	22
Figure 5.	The Effect of Initial α-Pinene Concentration on Ozone Production	23
Figure 6.	The Effect of Initial 1-Hexene Concentration on Ozone Production	24
Figure 7.	The Effect of Initial Cyclohexene Concentration on Ozone Production	25
Figure 8.	The Effect of Initial 1-Dodecene Concentration on Ozone Production	26
Figure 9.	The Effect of Initial M-Xylene Concentration on Ozone Production	27
Figure 10.	The Effect of Initial 1,3-Hexadiene Concentration on Ozone Production	28
Figure 11.	The Effect of Initial NO_2 Concentration on Condensation Nuclei from α-Pinene	31
Figure 12.	The Effect of Initial α-Pinene Concentration on Condensation Nuclei Production	32
Figure 13.	The Effect of Initial 1-Hexene Concentration on Condensation Nuclei	33
Figure 14.	The Effect of Initial 1-Dodecene Concentration on Condensation Nuclei	34
Figure 15.	The Effect of Initial M-Xylene Concentration on the Production of Condensation Nuclei Both With and Without SO_2 Present	35
Figure 16.	The Effect of Initial 1,3-Hexadiene Concentration on Condensation Nuclei	36

LIST OF FIGURES (continued)

		Page
Figure 17.	The Production of Condensation Nuclei from 1-Dodecene with SO_2 Present as a Function of 1-Dodecene Concentration	37
Figure 18.	The Effect of SO_2 on Condensation Nuclei Production from 1,3-Hexadiene	39
Figure 19.	The Effect of NH_3 on Condensation Nuclei Production from 1-Hexene	40
Figure 20.	The Effect of NH_3 on Condensation Nuclei Production from 1-Dodecene	41
Figure 21.	The Effect of NH_3 on Condensation Nuclei Production from M-Xylene	42
Figure 22.	Infrared Spectrom of Aerosol Produced by Irradiating α-Pinene and NO_2 in Dry Air	46
Figure 23.	Infrared Spectrum of Aerosol Produced by Irradiating 15 ppm of 1-Dodecene and 0.8 ppm of NO_2 in Dry Air	47
Figure 24.	Infrared Spectrum of Aerosol Produced by Irradiating 50 ppm of 1-Hexene, 0.8 ppm of NO_2 and 2 ppm of NH_3 in Dry Air	48
Figure 25.	Ozone Production as a Function of Hydrocarbon Concentration for Various Hydrocarbons Irradiated in Dry Air Containing 0.8 ppm NO_2	51
Figure 26.	Condensation Nuclei Production as a Function of Hydrocarbon Concentration for Various Hydrocarbons Irradiated in Dry Air Containing 0.8 ppm NO_2	53
Figure 27.	Dependence of Condensation Nuclei on O_3 Concentration with Fixed α-Pinene	58
Figure 28.	Dependence of Light Scattering Aerosol Upon Peak Ozone Concentration as Observed at Various Places in California During the California Aerosol Characterization Experiment	59
Figure 29.	Comparison of True and Apparent Dilution Curves	64

LIST OF TABLES

		Page
Table 1.	A Summary of Condensation Nuclei Results in Dry Air	20
Table 2.	Summary of Conditions for α-Pinene Experiments	21
Table 3.	Ozone and Nuclei Production Data for Toluene and 1,5-Hexadiene	30
Table 4.	Data on the Effect of Water Vapor at 50% Relative Humidity	43
Table 5.	Filter Collections of Aerosol Samples	45
Table A.	Comparison of True and Apparent Dilution Curves	63

SC551.17FR

THE FORMATION OF AEROSOLS IN A PHOTOCHEMICAL FAST FLOW REACTOR

ABSTRACT

This report details work performed on the study of aerosol formation in a photochemical fast flow reactor which may be operated in a "wall free" mode. During the period covered by this report, a new reactor was designed, constructed, and tested. Aerosols have been produced in this reactor in irradiated dry air containing typically 0.8 ppm NO_2 and 10 ppm of one hydrocarbon. The hydrocarbons studied were α-pinene, 1-hexene, cyclohexene, 1-dodecene, toluene, m-xylene, 1,3-hexadiene, and 1,5-hexadiene. The effect of the addition of various mixtures of SO_2, H_2O and NH_3 to the reactions was studied. Ozone and condensation nuclei concentration were measured in the reactor as a function of reactant concentration. Total mass production was measured by filter collection, and infrared spectra of some of the samples have been obtained.

Of the hydrocarbons studied, the olefin and diolefin compounds are more active than aromatics as nuclei formers. The olefin aerosol collected contained substantial amounts of oxygenated organics. With α-pinene, there was sufficient data to show a linear correlation between ozone production and aerosol formation. In addition, gases such as SO_2 and NH_3 increase condensation nuclei production. In the limited number of cases tried, water vapor at 50% relative humidity decreased or eliminated aerosol production from olefins.

1. INTRODUCTION

Aerosol formation continues to be one of the most important manifestations of air pollution in urban areas. The aerosols in urban areas have been subject to increasing study in the past several years.[1] In addition, laboratory experiments have been undertaken to study the formation mechanism of these aerosols.[2,3,4] However, the details of mechanisms of formation and growth of airborne particles in polluted atmospheres remains poorly understood. The present report is based on a previously developed[5] novel approach to studying mechanisms of aerosol formation in the atmosphere. Several important new results from this method are presented.

The first year report covered a feasibility study performed under CRC-APRAC contract. The first year objectives were to (a) determine if light scattering airborne particles can be produced in an air flow containing hydrocarbon vapors and nitrogen oxides, (b) analyze such particles for their chemical composition, and (c) determine the feasibility of using a flow reactor for simulation of photochemical generation of aerosols in polluted atmospheres. A flow reactor was designed, constructed, and tested for the production of aerosols in controlled experiments. The main goal was the generation of aerosols in the reactor in an irradiated mixture of NO_x, air, hydrocarbons, and possible additional trace components. Aerosols were observed in system: NO_2, air, 1-Hexene, SO_2, and H_2O system. However, attempts to produce aerosols with only NO_2, dry air, and an olefin irradiated in the flow reactor, with residence times of a few seconds did not produce aerosols.

The aerosols produced in the SO_2, 1-Hexene, NO_2 system were collected and analyzed for composition. These analyses included (a) $SO_4^=$, which was definitely present, (b) NO_3^-, which was detected but may have a contamination problem in the collection method, and (c) total organics, which were less than a few micrograms in a 100 µgm sample. Techniques for chemical analysis were also tested on organic aerosols produced in another reactor from pure ozone-olefin reactions in dry air.

This report covers the second year of effort under the CRC-APRAC* program to study the formation mechanism and composition of photochemical aerosols produced in a fast-flow reactor. The objectives of this study are to: 1) investigate the formation of aerosols in a photochemical fast-flow reactor using mixtures of HC, NO_x and air; 2) analyze the particles formed for their chemical composition to determine the role of organic material and nitrogen-containing material in the formation of aerosols, and 3) analyze and interpret the data obtained in 1 and 2, considering (a) mechanisms for photochemical formation of aerosols from gaseous atmospheric pollutants, (b) rate data for the transformation of trace gases into condensed phase, (c) material balance and products and (d) formation and behavior of aerosols in the actual polluted atmosphere.

Because of the critical importance of the first objective in the successful completion of the study, priorities were placed on this activity, with more limited effort on objectives 2 and 3.

The flow reactor employed maintains laminar flow in an irradiated section with a residence time in the neighborhood of ten seconds. The object of using a laminar flow reactor is to investigate aerosol forming reactions under controlled, steady flow, while minimizing the interaction of the walls with the reacting gases. The philosophy of this method has been described previously in the final report for the first part of this effort.[5]

The work described in this report had three distinct phases. Initially, experiments were carried out in extension of the work using the existing flow reactor employed in the previous contractual year. On the basis of these experiments, a new reactor was constructed. With the new reactor, a second series of experiments were carried out.

---

*CRC-APRAC is under the Air Pollution Research Advisory Committee of the Coordinating Research Council. Financial support was provided by the American Petroleum Institute, Motor Vehicle Manufacturers Association, and the Environmental Protection Agency.

Employing the first prototype reactor, experiments were carried out on the measurements of gas phase reactions, emphasizing the detection and formation of ozone in the reactor. These were followed by a series of experiments attempting to visualize the flow pattern in the reactor and characterizing the effects on the flow of various experimental parameters. Several experiments were carried out to investigate aerosol formation in the reactor. With the addition of ozone, experiments were carried out in the reactor to determine the range of reactant conditions required for aerosol formation. The experiments carried out led to the conclusions that although the probing methods were correct and the flow was essentially that expected, serious flow problems would occur in the reactor due, in particular, to thermal gradients. Condensation nuclei could be formed in an extremely short period of time if the ozone level was raised above that produced by irradiation alone. However, residence times of at least ten seconds were required to achieve useful levels of aerosol formation. On the basis of these factors, a new reactor was designed and constructed.

A new reactor was designed to allow longer residence time and better thermal stability of the flow for these experiments. The new design has a significantly larger radius and was continuously water-jacketed over not only the entire irradiation section but the flow development section as well. In addition, this reactor was supported by improvements in flow control and mixing. Experiments with this reactor show that much more stable laminar flow could be produced than with the previous reactor. In addition, with the new reactor, aerosols were formed without addition of ozone from various hydrocarbons and NO_2 in air at concentrations below 10 ppm.

With the new reactor, an experimental program to study condensation nuclei formation was carried out with eight different hydrocarbons, including 1-hexene, cyclohexene, toluene, m-xylene, 1-dodecene, 1,3-hexadiene, 1,5-hexadiene, and α-pinene. With the exception of toluene, varying concentrations of condensation nuclei were found for all hydrocarbons.

The effect of each hydrocarbon on the ozone production in the reactor was measured as a function of hydrocarbon concentration at a fixed NO_2 concentration. In the case of α-pinene, the effect on ozone production was also measured as a function of NO_2 concentration at a fixed α-pinene concentration. In addition to these experiments, several systems were studied with various combinations of SO_2, NH_3, and water vapor added to the reactant mixture.

The most striking feature of the data was that each system produced different results although some consistent patterns could be discerned. In each case, there was a hydrocarbon concentration at which production of nuclei increased dramatically. In addition there is a plateau region where the nuclei concentration changes little for increasing hydrocarbon concentration. Over the range of hydrocarbon concentrations studied, however, the ozone production varied dramatically. In some cases, the ozone production increased over the entire span of hydrocarbon variation. In other cases, ozone reached a peak at high hydrocarbon concentration or decreased over most of the hydrocarbon concentrations examined. In all cases where SO_2 was added, the condensation nuclei production increased; however, the concentration levels at which this was achieved varied dramatically from as low as six parts per billion to as high as 100 ppb. The introduction of ammonia at 5-10 ppm concentration increased the condensation nuclei number in each case it was tried. On the other hand, for the two olefins with which it was added, water vapor at 50% relative humidity decreased or eliminated aerosol formation.

For many of the cases studied, aerosol samples were collected on filters. Typically, 30-125 micrograms of condensed material were collected on these filters. For three of these cases, aerosols produced with α-pinene, aerosols produced with 1-dodecene, and aerosols produced with 1-hexene and ammonia, infrared spectra were obtained from samples extracted from these filters. These spectra show the presence of carbonyl compounds and possible C-O linkages as well as possible organic nitrates.

These data are presented in detail in this report and interpreted as they apply to atmospheric processes.

2. EXPERIMENTAL PROGRAM WITH THE PROTOTYPE REACTOR

We will refer to the reactor used in the first year effort as the prototype reactor to differentiate it from the new reactor constructed during the year covered by this report. To evaluate the prototype reactor at the start of the second year effort, several measurements were carried out to determine its performance and applicability to the study of aerosol formation. The observation of low ozone yields relative to estimated light intensity led to a series of measurements of ozone in the reactor and to a separate physical measurement of the light intensity. In addition, smoke visualization of the flow pattern was carried out. Finally, aerosol experiments were performed, including both attempts to produce photochemical aerosols and to study the production of aerosols from ozone and olefin mixtures in the reactor.

2.1 Ozone Measurements

To determine the validity of the ozone measurements in the reactor, an ozone injector was added to the reactor with the lamps off. The level of ozone at the injector was measured with a REM ozone monitor and then as a function of distance in the reactor. In the range from 100 ppb to 3 ppm, no significant evidence was found for a loss mechanism. The ozone was constant as a function of distance in the reactor. Furthermore, measurements were made with a dilution probe with the total flow through the probe held constant at 700 cc/min. These are summarized in Figure 1.

In interpreting these curves, it is important to note that a bimolecular or higher order reaction in the probe will produce a non-linearity in the measured quantity as a function of dilution. The straight lines in this figure are "apparent theoretical dilution curves" assuming that there is no reaction taking place. If there are no dark reactions taking place, the y-intercept is the correct ozone concentration and the measured concentration as a function of dilution will follow the straight line. If there is another molecule present which is reacting with the ozone in the probe then the ozone concentration measured at zero dilution flow is incorrect and the measured

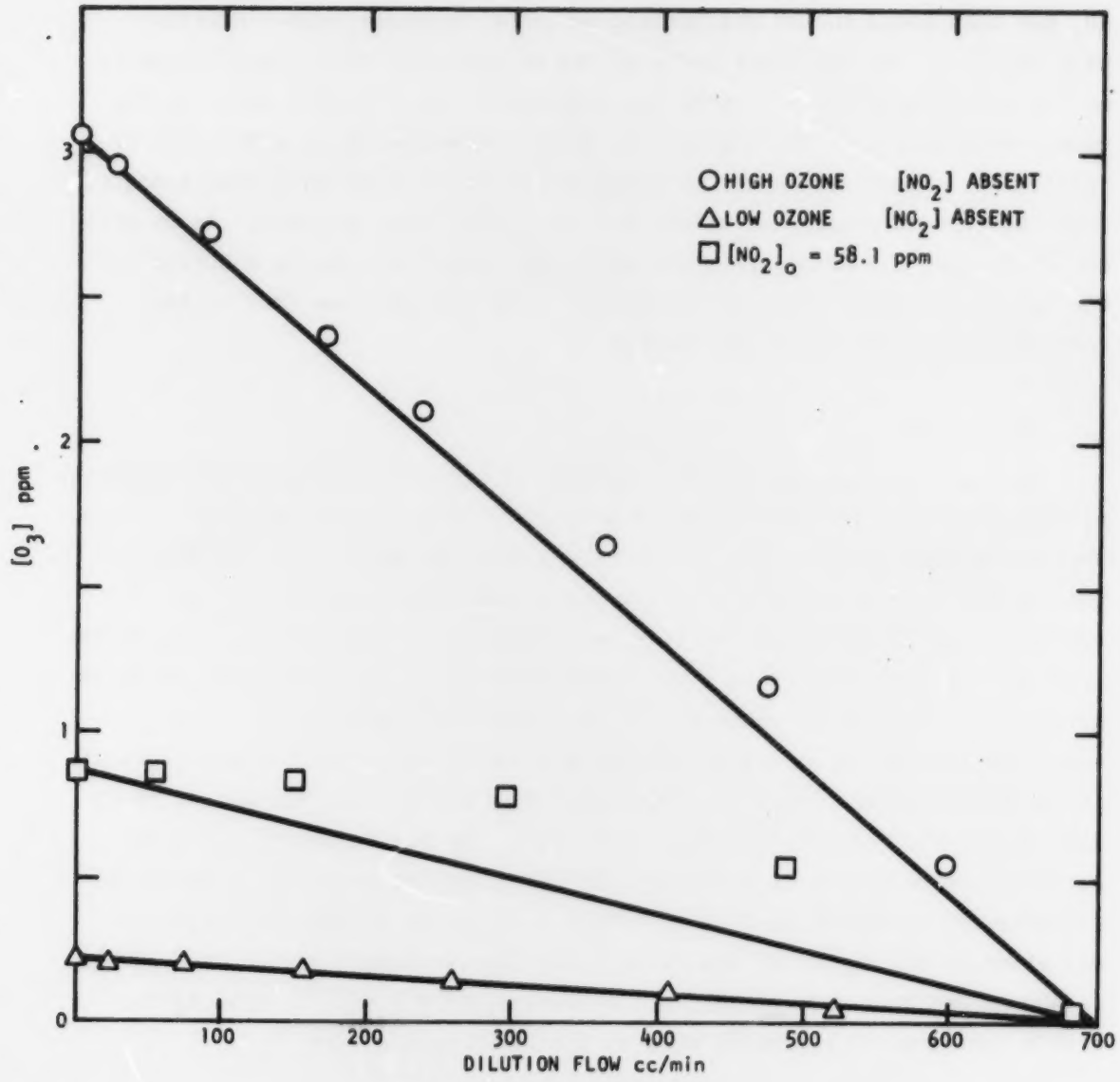

Figure 1. Ozone Measurements with the Dilution Probe in the Prototype Reactor

concentration as a function of dilution will be larger than given by the apparent theoretical dilution curve. This is explained more fully in Appendix A of this report. In the case of the center line of the figure, NO_2 has been added to the reactor and we see a deviation from linearity with dilution. On the lower curve we see no deviation from linearity while on the upper curve there is some non-linearity. As a further check on the ozone measurements in the reactor the ozone concentration as a function of initial NO_2 concentration was measured and found to agree with that expected from the currently accepted values for the O_3+NO_2 rate constant. As we will see in Section 2.3 below, this was partially fortuitous due to a spread in the actual residence times in the reactor. We may conclude that we are correctly measuring O_3 in the reactor.

2.2 Actinometry

To check on previous chemical methods of actinometry, the light intensity was measured with a Hewlett Packard Model 8334 Radiant Flux Detector. Since this instrument measures the flux incident on a surface, it is difficult to measure the more meaningful volume density which determines k_d for NO_2 for our geometry. We measured the flux as a function of angle on the axis of the cylinder. In the direction of the lamps there is 20 milliwatts/cm^2 while in all other directions an average of 8 milliwatts/cm^2, which when integrated about 360° yields an equivalent of 324 milliwatts/cm^2. Approximately 36% of the intensity of the lamps (in the region detected by the flux meter) is at wavelengths which dissociate NO_2. Therefore, the equivalent of 117 milliwatts/cm^2 of radiation is available for the dissociation of NO_2. Using the estimates of Leighton[6] we find that this is about 10.6 times the actinic radiation of the sun at 0° zenith angle in the wavelength region from 300 nm to 400 nm and thus corresponds to a k_d for NO_2 of 4.7 min^{-1}. This falls within the range of estimates made in the first year effort.[4]

2.3 Flow Visualization

The flow in the reactor was visualized by injecting cigarette smoke at one point in the flow or by adding a smoke pulse to the total gas flow. The

quality of visualization that could be achieved is shown in Figure 2.

One problem with using cigarette smoke is that the smoke aerosols are suspended in a parcel of gas which contains a large proportion of CO_2. Thus, the bulk density of this smoke parcel is much greater than the air density and consequently the smoke tends to fall. If the Reynold's number of the flow is high enough, the smoke parcel will appear to be moving along with the flow, the fall velocity being much smaller than the gas flow velocity. However, as the flow velocity decreases, then the fall velocity will become a much more significant factor. For the prototype reactor design, the velocity was high enough so that the smoke settling was not a problem. In this case, the flow profile could be photographed (Figure 2) and through this technique, it was found that the end of the reactor was disturbing the flow. Thermal effects could also be visualized by heating the wall of the reactor and watching the thermal eddies produced in the flow. A temperature differential of less than 1°C was enough to produce thermal instabilities.

An attempt to measure the residence time with a smoke pulse from the ozone injector showed that a large spread in residence time occurred. With a nominal 5 second residence time the first visible smoke reached the probe in three seconds and there was still smoke arriving at 20 seconds. It is for this reason that the O_3+NO_2 observations are considered fortuitous.

2.4 Aerosol Experiments with the Prototype Reactor

During the first year of effort, with the prototype flow reactor, aerosols were produced from irradiated mixtures in air of NO_2, SO_2 and either 1-butene or 1-hexene, all at large concentrations ($\geq$10 ppm), as well as water vapor. No aerosols were produced with only 1-butene or 1-hexene, NO_2 and air, and no organic material was found in the sulfate aerosols. Since the main thrust of the present program was to study organic material in aerosols, two experiments were carried out with the reactor to ascertain the possibilities for organic aerosol formation.

First an attempt was made to produce aerosols with α-pinene. The NO_2 concentration was varied from 0 to 120 ppm and α-pinene was run at 15 ppm

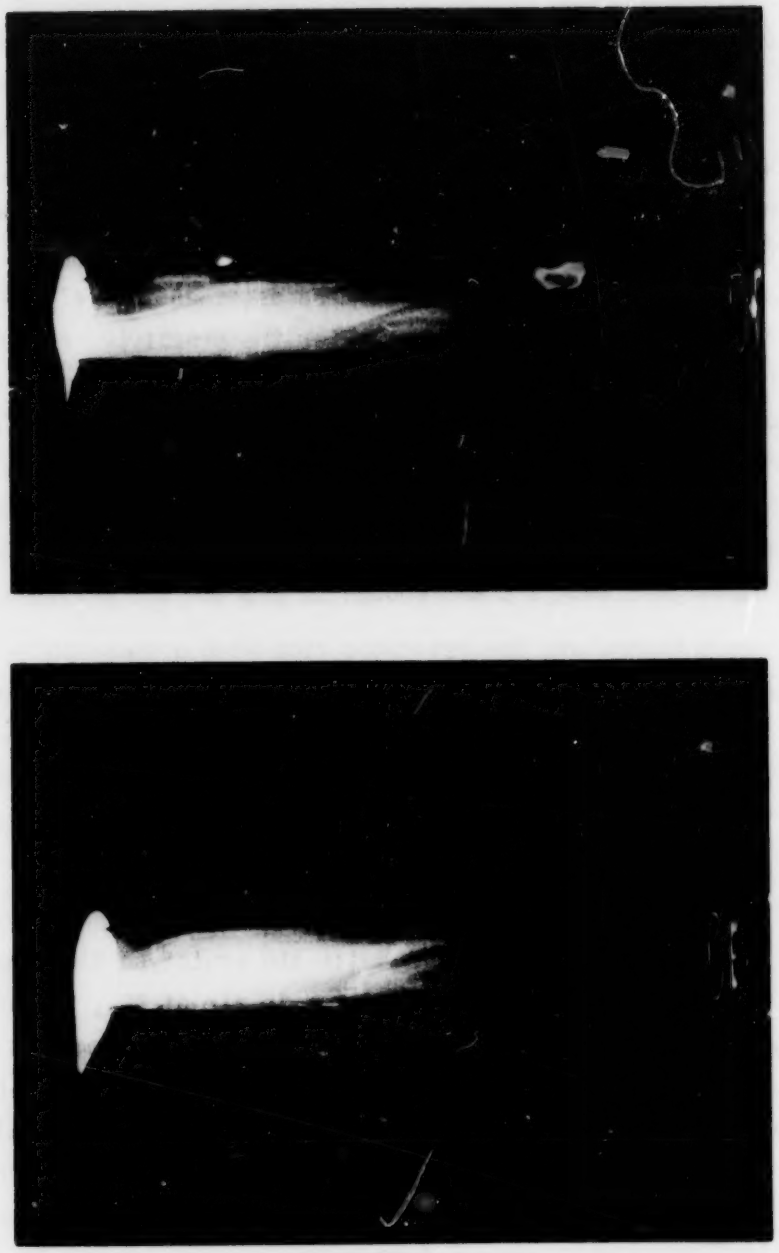

Figure 2. Smoke Visualization of Flow in Prototype Reactor.
Top with Input Screens, and Bottom Without.

and 126 ppm. The residence time in the irradiated section was either four or eight seconds. Under these conditions, the ozone level was never more than 0.04 ppm, and no aerosol was observed with the condensation nuclei counter. To determine what factors were involved in the absence of aerosols, a new experiment was performed. A nozzle was placed in the reactor at the beginning of what would normally be the irradiated section. With the lamps off, ozone was added to the reactor through the nozzle with 1-hexene present. With 2.2 ppm of ozone present and 10 ppm of 1-hexene, aerosols were formed and their concentration increased with increasing 1-hexene concentration. A measurement of nuclei concentration as a function of distance along the reactor showed that aerosols were produced with increased concentration downstream, and their number reached a plateau of 10^4 per cc after 5 cm, which was less than two seconds residence time. However, when NO_2 was added to the ozone/hydrocarbon mixture, the behavior became very complex. During each run, when NO_2 was added, the aerosols initially increased then gradually decreased until none were produced. This was true at a level of from 0.5 ppm to 10 ppm of NO_2. For NO_2 concentration of 0.1 ppm, there was still a decrease in aerosols after long times, but there was a steady-state concentration of nuclei. The time required to reach steady state in either case was longer than any characteristic gas mixing time in the reactor. The effect has remained unexplained as to whether it is a reactor artifact or some other phenomenon.

2.5 Conclusions on the Prototype Reactor

The conclusion reached from the data presented above was that a new reactor with improved design was needed. In particular, the problems of flow stability and the need for a longer residence time were considered important factors for successful study of aerosol generation. There was evidence in the flow visualization measurements that thermal gradients were a serious limitation and attention to better heat control by water jacketing was required. As we found later (see Section 3.1.3), from flow visualization measurements in the new reactor, control of thermal gradients is of the utmost importance. The light intensity was judged to be adequate on the

basis of the experiments performed. Thus, it was decided to construct a new, larger diameter reactor with improved temperature control and flow development.

3. THE NEW REACTOR SYSTEM

3.1 The New Reactor

As a result of the studies discussed in Section 2, a new flow reactor with a larger inside diameter and a continuous water jacket was constructed. This reactor allowed the use of longer residence times without compromising the wall-free nature of the reactor, as explained below.

3.1.1 Flow Theory for the New Reactor

In order to demonstrate the relation between reactor size and wall-free operation, we refer to page 29 of our previous CAPA-8 report[5] where we show, that for a given level of diffusional contamination from the wall,

$$t = \sigma a^2$$

where t = residence time in the reactor
a = radius of the reactor
σ = constant determined by the allowable level of contamination.

If we increase a by a factor of 3, then the allowable residence time will increase by a factor of 9. On page 30 of the same report,[5] the Reynolds number is shown to be inversely proportional to a if t satisfies the above relationship, so the Reynolds number decreases and the flow is more stable against the onset of turbulence.

Thus, by increasing the radius of the reactor we increase, in proportion to the square of the radius, the time in the reactor that it takes for material to reach the probe from the walls. The residence time can then be increased without changing the wall-free nature of the reactor.

Although the new design will be more stable against the generation of turbulence, thermal convection becomes a more critical factor. Stability

against thermal convection is proportional to the Grashof number[7]

$$G = \frac{B\Delta T g L^3}{\nu^2}$$

where B = volume expansion coefficient of air
ΔT = the variation of temperature in the system
g = gravitational constant
L = characteristic radius of the system
ν = kinematic viscosity of air.

As we increase the radius of the reactor, the Grashof number is increased as the cube of this size, thus dramatically increasing the probability of thermal convection. This is important since it limits relative size of the reactor. For our case we are interested in the magnitude of the convection relative to the flow in the reactor. Thermal convection is proportional to a power of the Grashof number.[8] Since the flow velocity has also been decreased as the square of the radius, the relative importance of thermal convection increases rapidly with the radius of the tube. The effects of thermal convection on flow stability were explored explicitly using the smoke flow visualization method.

3.1.2 The New Reactor Design

Figure 3 shows a diagram of the new reactor. It consists of a main 2.4 metre section, a 15 cm probe section, a 1.2 metre outlet section, and a gas input system. The main reactor section is composed of two concentric pyrex tubes. The inner tube is 15 cm I.D. and the outer one is 18.8 cm O.D. The outer tube is about 20 cm shorter than the inner. They are held in place by a plastic ring at each end to which they are sealed with RTV Silastic cement. Water is admitted to the space between them through the plastic rings. The lamp housing is the one used previously with a slightly larger opening to accept the water jacket. The illuminated section is still nominally 20 cm long and is centered approximately 30 cm from the output end of the water jacketed section. Due to necessity during construction, the input end of the reactor is reduced to 12 cm O.D. This occurs beyond the water jacket.

SC551.17FR

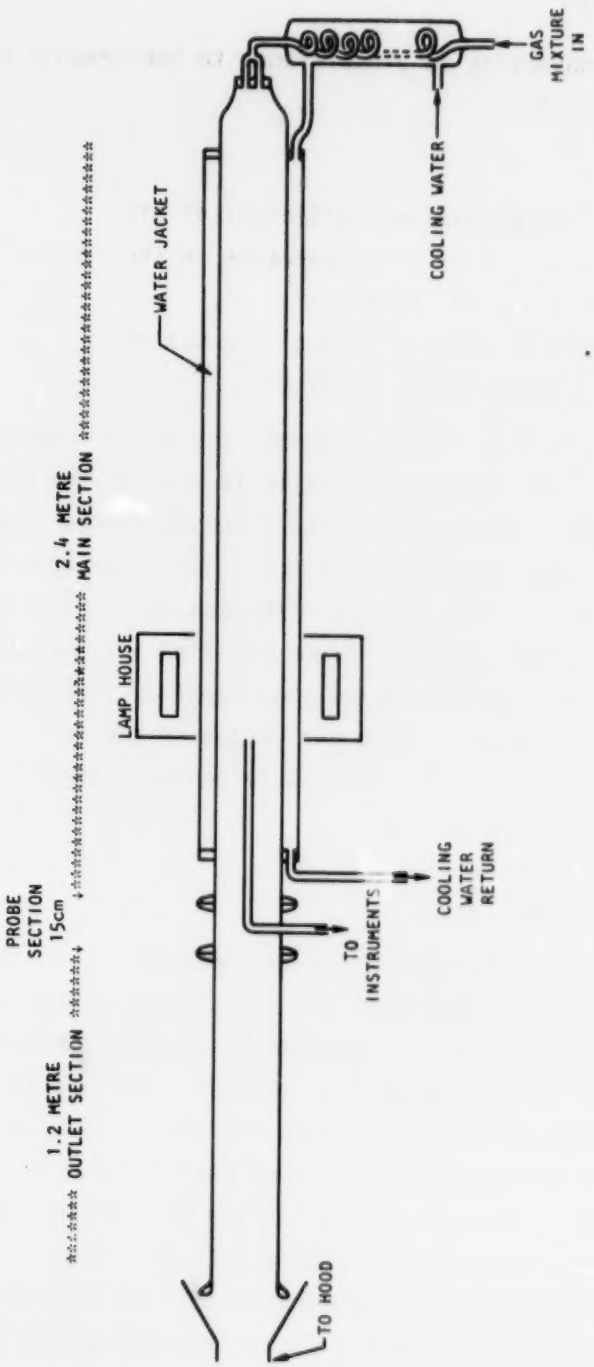

Figure 3. Scale Diagram of the New Reactor

The gas mixture is introduced at this end through four 0.6 cm holes in a stainless steel flange. Before reaching this flange, the gas is equilibrated to the reactor temperature by passing through a spiral condenser in whose water jacket the reactor cooling water flows.

For all of the experiments described below a fixed probe was employed. It was 1 cm in diameter and 6 cm beyond the end of the illuminated section. The probe then passes out of the reactor through the wall of the 15 cm section. This section is followed by the 1.2 metre end section, the purpose of which is to keep end disturbances away from the probe. The output of this last section flows into a conical hood.

3.1.3 Flow Visualization in the New Reactor

In the new reactor, the flow velocity is much lower than in the prototype. Since the smoke parcels are laden with CO_2 as well as smoke they are heavier than the air in the reactor. At the new lower flows the viscous forces are less than the gravitational force causing the parcels to fall. This was alleviated by filling the reactor with very dilute smoke. The individual smoke particles are light enough so that the viscous forces dominate and the particles follow the flow closely. The flow was illuminated with a small He-Ne laser.

The smoke particles scattered the laser light and they could be observed visually with the aid of a magnifying glass. Since the amount of light was very limited, no photographs could be taken. However, the relative velocity of the particles could be judged visually.

It was observed that at a total flow below 7 1/min (residence time 15 sec) a counterflow developed through part of the reactor. In other words, at a given plane perpendicular to the flow, some of the material was flowing back in the opposite direction. This effect was shown to be generated by temperature differences within the reactor. Even with the reactor walls and inlet gas kept at a constant temperature, the flow could not be stabilized. Five meshed nylon screens mounted at the ends of the reactor were tried, but this also had no stabilizing effect. However, when the flow rate was in-

creased above 7 1/min, the viscous forces overcame the thermal effects and the flow stabilized into a laminar streamline flow. This effect was seen with the laser by observing the particles moving much faster in the center of the reactor than at the edges. This study placed a minimum operating flow rate of 7 1/min with the new reactor. However, even above 7 1/min, the thermal stabilization was still required because local heating of the wall destabilized the flow.

An end effect was also observed with the new reactor, and an additional 120 cm of glass pipe at the end, shown in Figure 3, corrected this problem.

3.1.4 Advantages of the New Reactor

The new reactor system has the following advantages over the prototype system: a) longer residence times may be achieved for the same wall-free effect, b) the flow development and irradiated sections are continuously water jacketed with no thermal gradient from one to the other, c) there is no physical flow disturbance from the beginning of the flow development section through the irradiated section, d) the input and output flows are better stabilized and input and output disturbances do not propagate into the irradiated section, and e) there is no spread in residence times.

3.2 Modifications in the Gas Handling System

Several changes have been made in gas mixing systems to improve stability, gas purity, and convenience. Those gases which are provided at low pressure through the Science Center building supply system (oxygen, nitrogen) are regulated by Matheson Model 70 pancake regulators. The NO_2 in nitrogen is regulated by a Veriflow Model IR300 regulator. Except for 1-hexene, all hydrocarbons were added by saturating dry nitrogen at a controlled temperature, either in an ice bath or in a regulated constant temperature bath. Except for a dilution flow above the hydrocarbon saturator, all other flows were measured with Tylan FM-400 mass flow meters. The outputs of these flow meters were displayed digitally on a unit which could be switched from one flow meter to another and values read out in physical

units. This provided exceptional convenience in carrying out a variety of experiments. The flow meters were calibrated with bubble flow meters and a wet test meter, depending upon the range required.

4. EXPERIMENTAL PROCEDURES

The data presented in Section 5 were collected in three distinct steps; 1) for each case, condensation nuclei and ozone were measured as a function of concentrations of various reactants, 2) filter samples were collected and, 3) the filter samples were extracted and analyzed. The procedures for each phase will now be described.

4.1 Ozone and Condensation Nuclei Measurements

For each hydrocarbon considered, the production of condensation nuclei was investigated over a range of hydrocarbon concentrations beginning with a few ppm. The onset of nuclei varied with hydrocarbon, but once it was observed, the concentration of hydrocarbon was then increased gradually. At each concentration, a period of time from 5 to 30 minutes was allowed before measurement to insure a stable valid value. In those cases, as described below, in which no stable value was obtained in 30 minutes, then an average value over the next 5 minutes was recorded. After each condensation nuclei reading, the probe output was switched for an ozone reading.

The condensation nuclei were measured with an Environment One condensation nuclei counter, and ozone was measured by a REM chemiluminescent ozone monitor. The probe flow output passed through a three-way valve so that one could switch from one instrument to the other. The nuclei counter required a flow of 2.1 liters/min while the REM required 1 liter/min. Both of these flows were in large excess over the isokinetic sampling flow; however due to installation difficulties, a dilution probe was not installed at this time and all of the data was collected with a simple 9 mm diameter probe. This was not expected to be a problem for particles as small as ours; however we do attribute some instabilities in formation of particles for some cases to the flow instability caused by the probe. A typical run is detailed

in Appendix B.

4.2 Filter Collections

The aerosol samples were collected on 25 mm Gelman Type A glass fiber filters in a standard Millipore filter holder. The filters were cleaned and dried by baking them at least overnight at 425°C. A regulated flow of 3 l/min was sampled from the probe through the filter for 16 hours (overnight). The level of the condensation nuclei was checked before and after the filter collections and found to be constant. The filters were weighed before and after collection on a Mettler Type MS microbalance.

4.3 Infrared Analysis

In order to extract the organic material from the filter, several extraction procedures were employed along with several different solvents. The solvents used included ethyl ether, ethanol, chloroform, and p-dioxane. The chloroform was shown to be the least reactive and produced the best background spectrum. The other solvents showed absorption of water vapor during the extraction process. This effect appeared as broad peaks in the 3500 cm^{-1} and 1660 cm^{-1} region of the IR spectrum, a region of interest for the organic samples.

There were two basic extraction techniques employed for the aerosol analysis: 1) some samples were washed by immersing the filter in a beaker filled with solvent at room temperature. Washing times ranged from five minutes to several days; 2) other samples were extracted for two to three hours using a 10 ml micro-soxhlet extractor. In both cases, about 20 cc of solvent was used. After the sample was dissolved in the solvent, it was concentrated, using dry N_2, to 0.25 cc and put into a liquid sampling IR cell.

The IR analysis was performed using a Perkin-Elmer 421 dual beam spectrophotometer. For normal operation, the instrument was run at an 8-minute scan speed with the attenuator at 1100 and the slits opened to their normal position. In some cases, the sample absorptions were so small that the 5X

scale expansion was used to increase the instrument sensitivity. In this mode, the scan speed was reduced to 32 seconds, the attenuator was reduced to 600 and the slits were opened to their X2 position.

5. RESULTS

The data obtained with the new reactor will now be presented in three separate parts, including condensation nuclei and ozone data in the first part, filter collections in the second part, and infrared analysis in the third.

5.1 Condensation Nuclei and Ozone Data

Table 1 summarizes the cases covered by the experiments in the new reactor. Eight different hydrocarbons were employed in mixtures of NO_2, SO_2, NH_3, H_2O and air. With the hydrocarbons taken one at a time and combinations of SO_2, NH_3 and H_2O, we have in all 64 cases, of which our experiments have covered 20 cases. The hydrocarbons selected cover a large range of types. There were two mono-olefins with 6 and 12 carbons respectively, 1-hexene and 1-dodecene; a C_6 cyclic olefin, cyclohexene; two light aromatics, toluene and m-xylene; two C_6 diolefins, 1,3-hexadiene, and 1,5-hexadiene, and finally α-pinene, a bicyclic monoterpene.

The data obtained with these hydrocarbons and NO_2 in the reactor with dry air will be presented followed by a description of the results of adding various other compounds.

The data which are presented in Figures 4 through 10 record the effect on ozone for each hydrocarbon as condensation nuclei were measured. This set of experiments was begun with α-pinene, and all the data obtained with α-pinene are presented in Table 2. Figure 4 is a graph of ozone production as a function of initial [NO_2] with α-pinene present. The result is not surprising; the ozone concentration increases linearly for low [NO_2] and increases less rapidly as the [NO_2] increases. The remainder of the ozone data show some important differences and a wide diversity. As seen in Figure 5, there is a dramatic peak in ozone production as a function of

TABLE 1

A SUMMARY OF CONDENSATION NUCLEI RESULTS IN DRY AIR

For all experiments shown concentration of NO_2 is 0.8 ppm.
One case is shown for each system studied.

	Concentration of Reactants			
Hydrocarbon	Hydrocarbon (ppm)	NH_3 (ppm)	SO_2 (ppb)	Nuclei Concentration (per cc)
1-Hexene	32	-	-	4.5×10^4
	17	9	-	7×10^4
Cyclohexene	15	-	-	*
1-Dodecene	30	-	-	2×10^5
	12	-	6	8×10^5
	13	4	-	4×10^5
	12	2.6	12	1×10^7
1, 3-Hexadiene	10	-	-	2×10^5
	7.5	-	11	1×10^6
1, 5-Hexadiene	70	-	-	1×10^4
α-Pinene	20	-	-	6×10^5
Tolune	23	-	-	0
M-Xylene	50	-	-	3×10^3
	50	-	100	1×10^4
	32	6	-	3×10^3

*Nuclei concentration varied with time for fixed experimental parameters. (See text).

TABLE 2

Summary of Conditions for α-Pinene Experiments

Run	Flow ℓ/min	Residence Time sec	[α-pinene] ppm	[NO_2] ppm	[O_3] ppm	CNC per cc
1	9.79	10.8	2.87	0.76	NM	150K
2	9.76	10.9	2.87	0.56	0.22	100K
3	9.72	10.9	2.98	0.54	0.25	100K
4	9.70	10.9	1.17	0.56	0.165	30K
5	9.46	11.2	0.56	0.56	0.13	1K
6	9.35	11.3	5.53	0.56	0.29	200K
7	9.25	11.5	9.1	0.59	0.22	240K
8	9.98	10.6	13.2	0.55	0.16	250K
9	9.98	10.7	19.9	0.57	0.10	650K
10	9.95	10.7	2.65	0.52	NM	100K
11	9.85	10.8	2.58	0.38	0.18	80K
12	9,82	10.8	2.58	0.177	0.125	50K
13	9.82	10.8	2.58	0.104	1.08	25K
14	9.67	11.0	2.63	0.036	0.03	0
15	9.62	11.0	2.55	0.074	0.05	20K

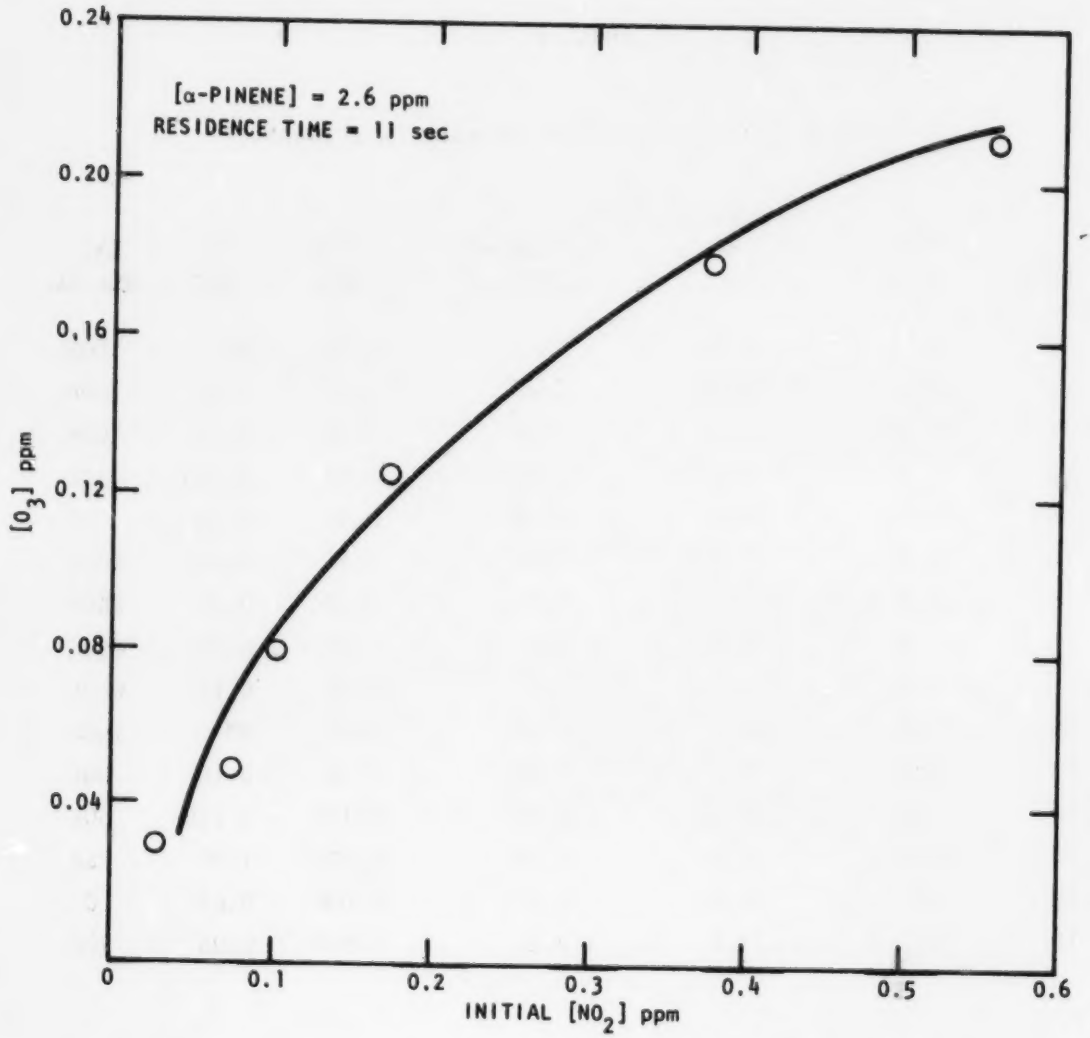

Figure 4. The Effect of Initial NO_2 Concentration on Ozone Production with α-Pinene.

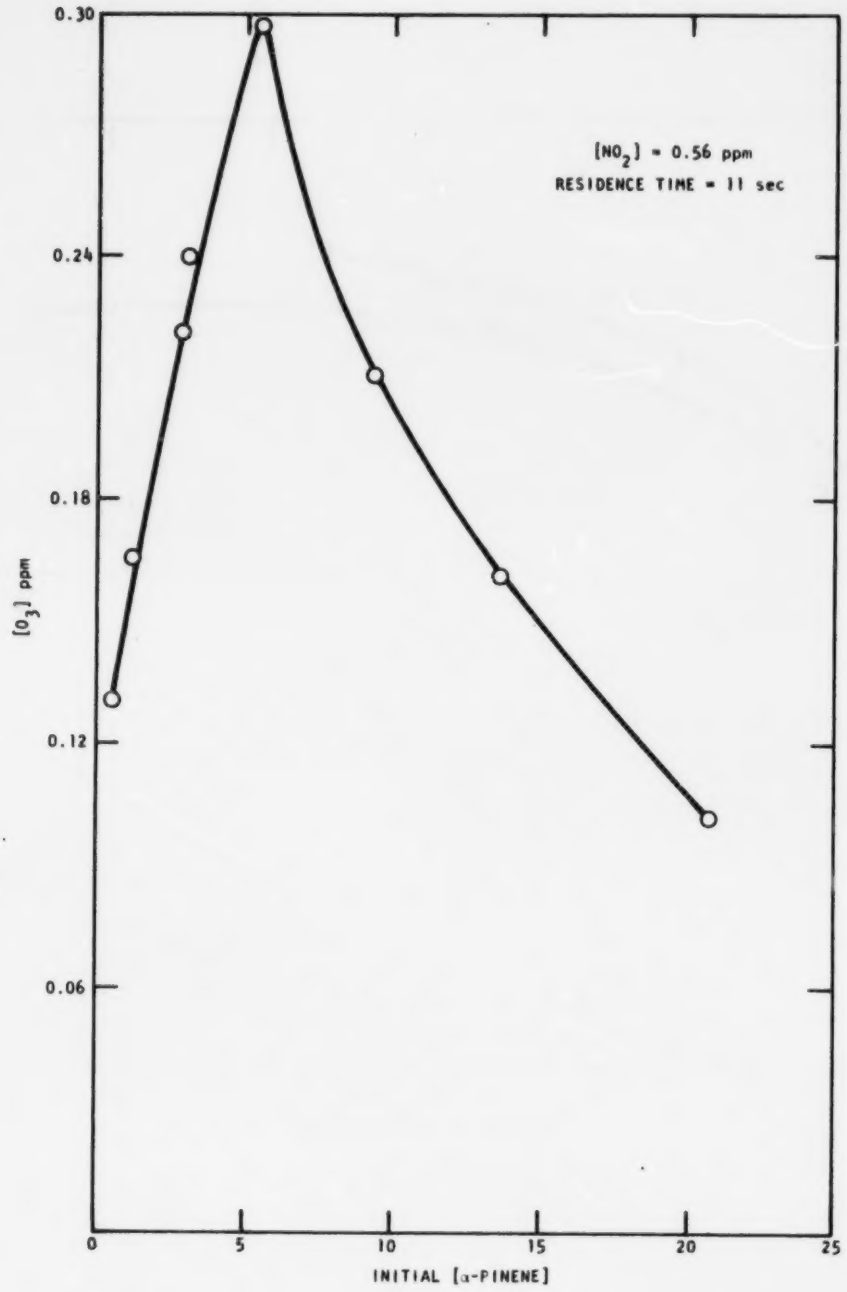

Figure 5. The Effect of Initial α-Pinene Concentration on Ozone Production

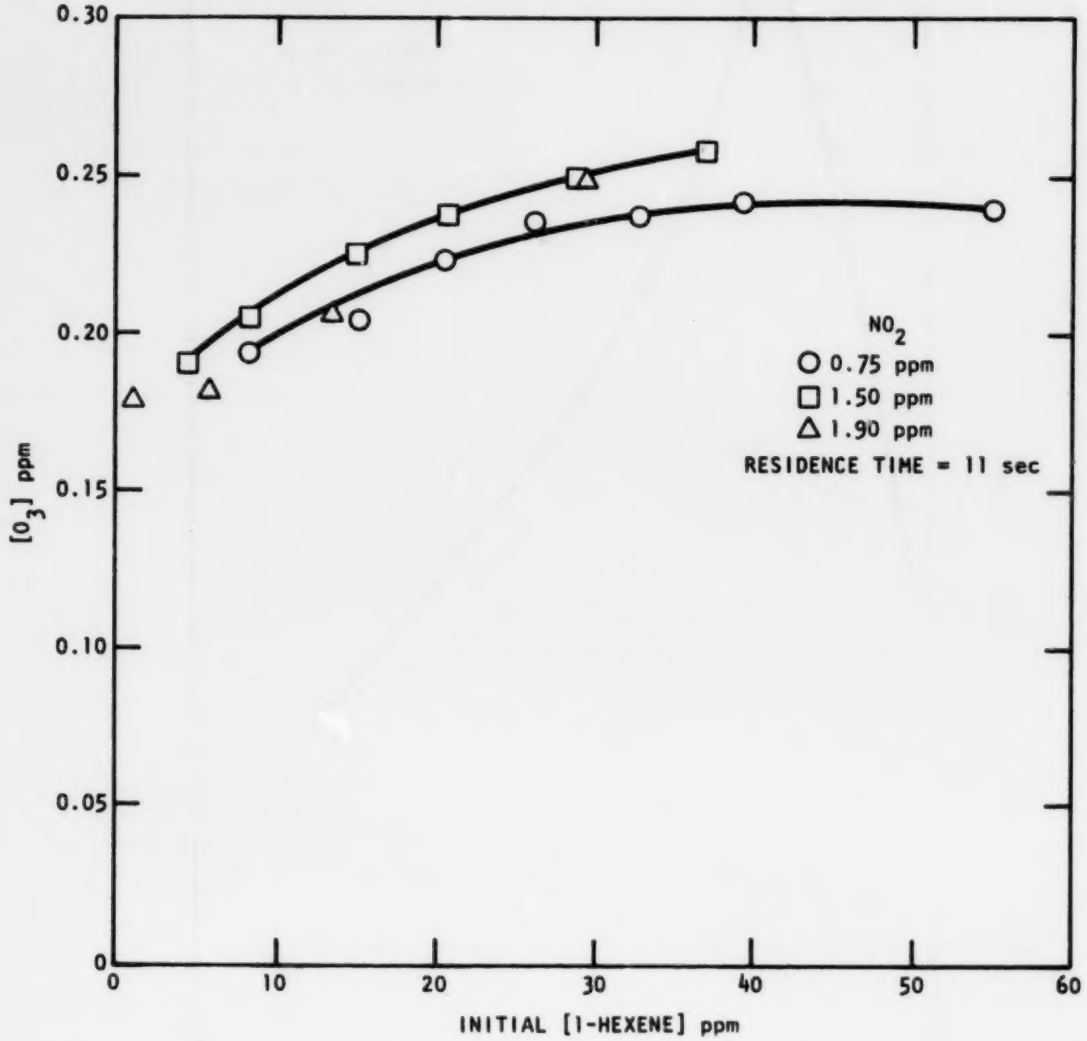

Figure 6. The Effect of Initial 1-Hexene Concentration on Ozone Production

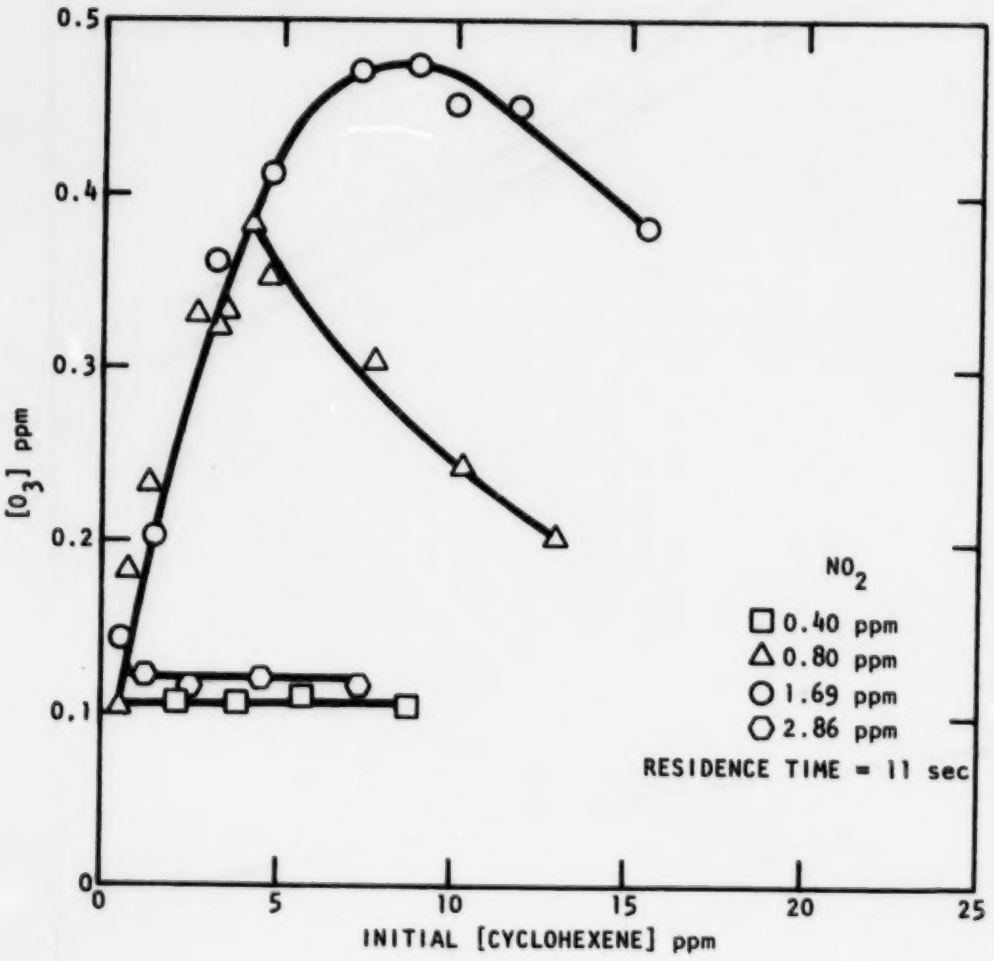

Figure 7. The Effect of Initial Cyclohexene Concentration on Ozone Production

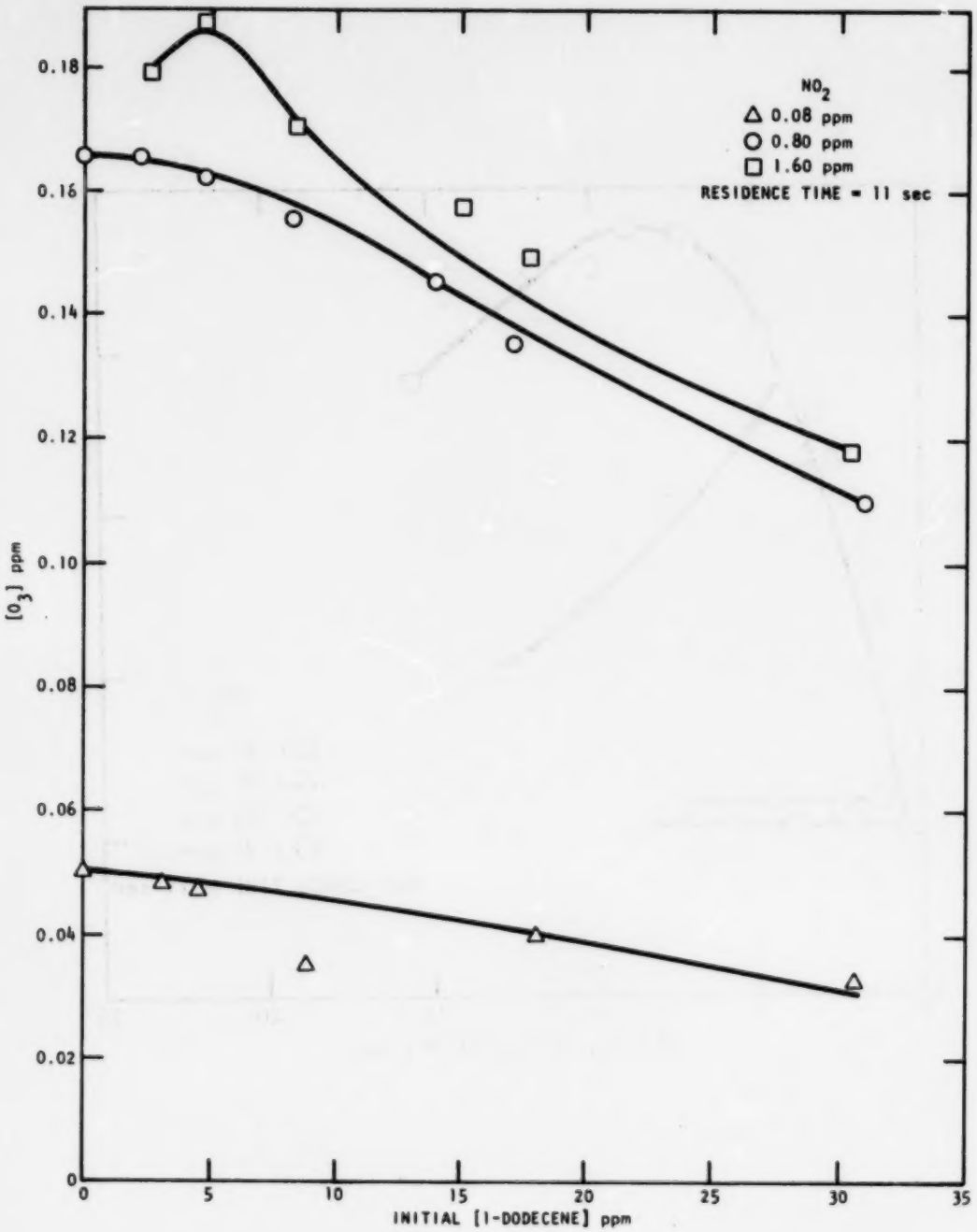

Figure 8. The Effect of Initial 1-Dodecene Concentration on Ozone Production

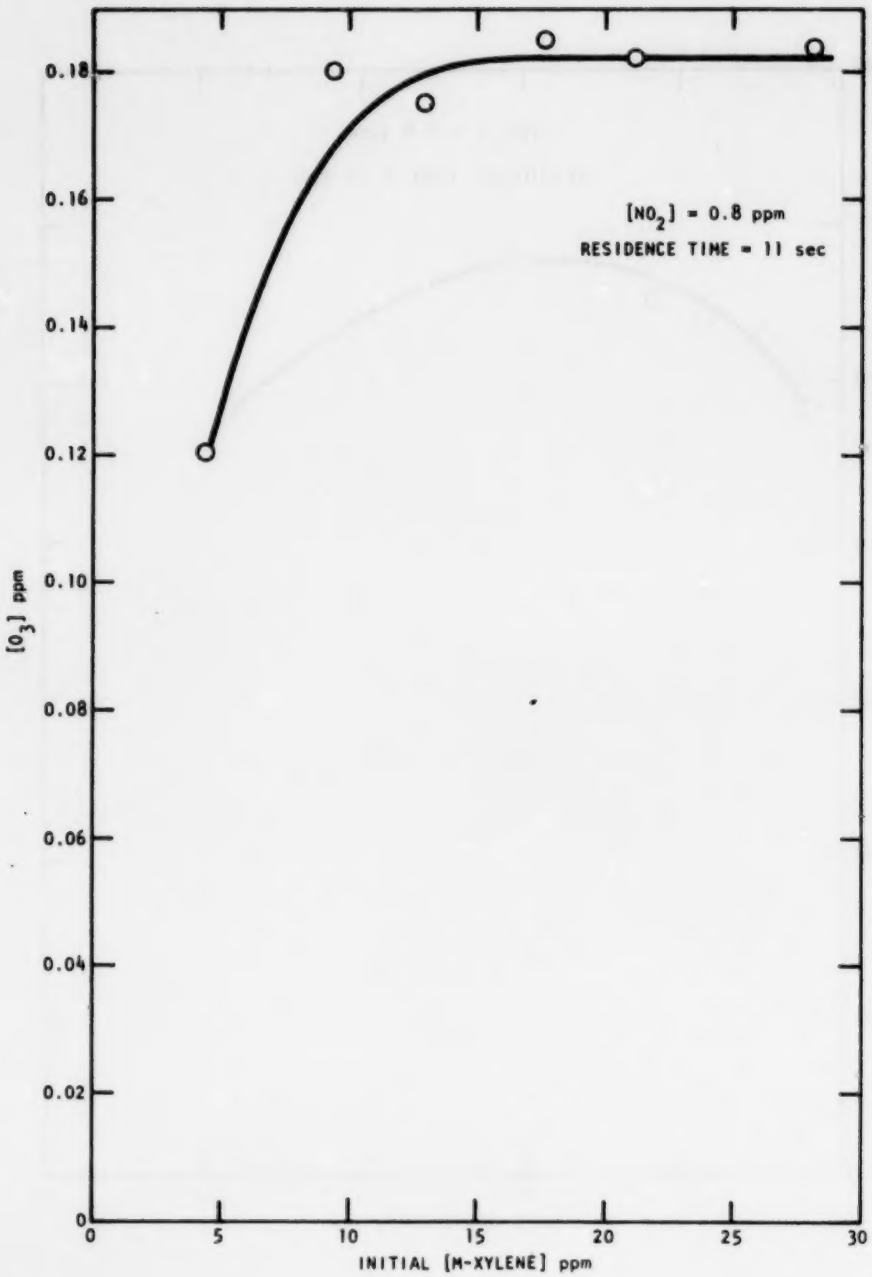

Figure 9. The Effect of Initial M-Xylene Concentration on Ozone Production

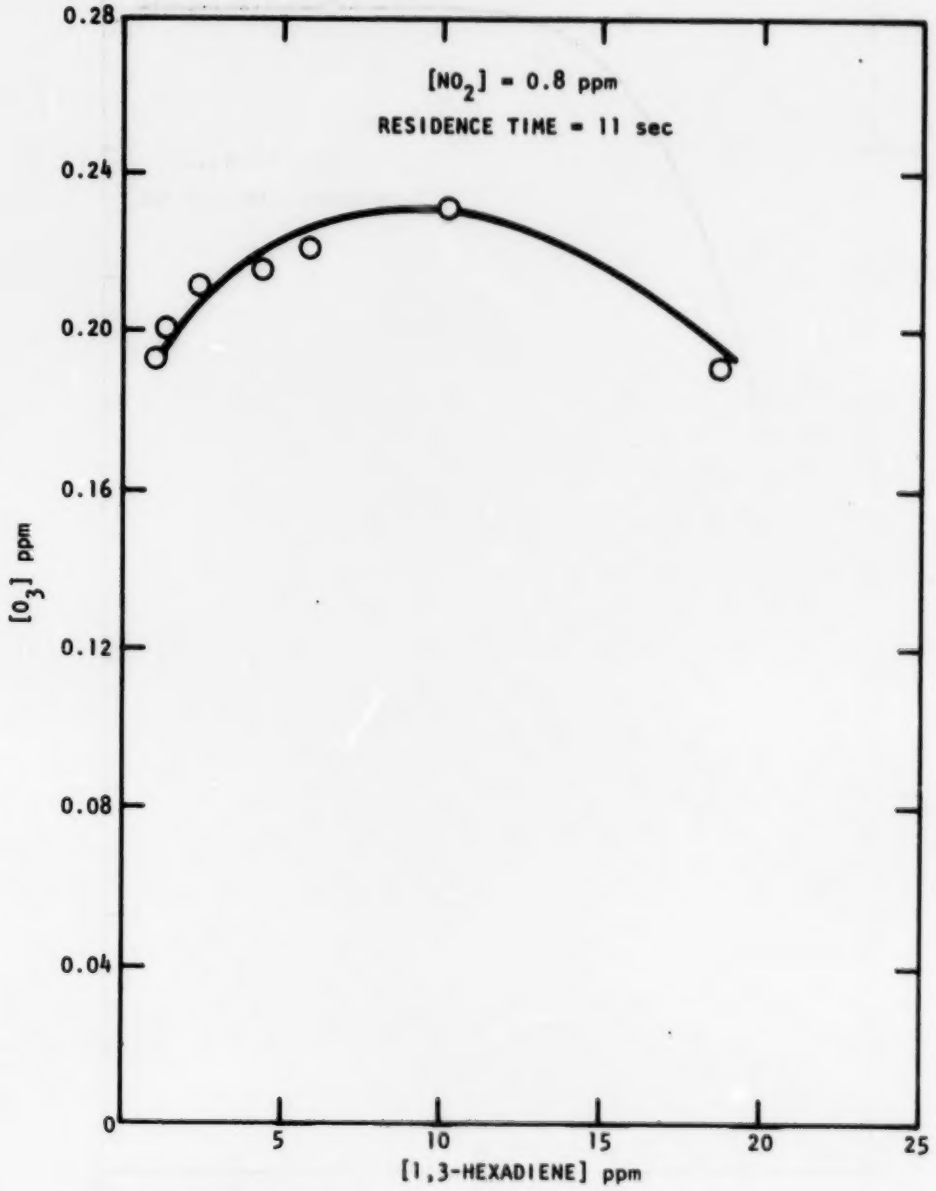

Figure 10. The Effect of Initial 1, 3-Hexadiene Concentration on Ozone Production

initial α-pinene concentration. This behavior is repeated less dramatically with cyclohexene in Figure 7, slightly with 1-dodecene in Figure 8, and perhaps also with 1,3-hexadiene in Figure 10. On the other hand, for 1-hexene in Figure 6, and m-xylene in Figure 9, we see only an increase. For 1,5-hexadiene (see Table 3), a decrease was observed for the one NO_2 concentration used. The effect of hydrocarbon concentration upon ozone production depends upon the NO_2 concentration for the cases of 1-dodecene and cyclohexene but not for 1-hexene. Finally, for toluene (see Table 3), the ozone concentration was independent of hydrocarbon concentration. Altogether, the ozone production data shows considerable diversity and, despite some patterns, each case appears different.

In the case of the condensation nuclei production, there was less diversity but some significant differences in behavior between systems were observed. With α-pinene the nuclei increased as the initial concentration of NO_2 increased as shown in Figure 11. This behavior is similar to that observed for ozone. This particular comparison will be discussed in Section 6. As initial hydrocarbon concentration was varied, the pattern (Figures 12 through 17) was the same for all hydrocarbons tested except toluene and cyclohexene. With toluene, no aerosols were obtained; with cyclohexene, the measurements were so unstable as to render quantitative measurement impossible; this will be discussed below. The remaining six hydrocarbons showed the same dramatic increase as hydrocarbon concentration increased, followed by a plateau or the beginning of one. The two major differences from one to another were the range of hydrocarbon concentration over which this took place and the concentration of nuclei reached on the plateau. The three most copious aerosol producers were α-pinene, 1-dodecene and 1,3-hexadiene, which reached $7x10^5$, $2x10^5$, and $2.5x10^5$ nuclei per cc respectively. In addition, all three exceeded 10^5 nuclei per cc by the time the hydrocarbon concentration reached 10 ppm. On the other hand, of those which produced measurable aerosols, m-xylene and 1,5-hexadiene (Table 3) produced the least, $3x10^3$ and $2x10^4$ nuclei per cc respectively, and these values occurred at hydrocarbon concentrations of 50 and 73 ppm respectively, which is above our range of interest for atmospheric application. 1-hexene at $5x10^4$ nuclei per cc had begun to reach its plateau, but this was at 53 ppm.

TABLE 3

OZONE AND NUCLEI PRODUCTION DATA FOR TOLUENE AND 1,5-HEXADIENE

All experiments performed in Dry Air Containing 0.8ppm NO_2

HYDROCARBON	HYDROCARBON CONCENTRATION (ppm)	OZONE PRODUCED (ppm)	NUCLEI CONCENTRATION (per cc)
Toluene	.27	.164	0
	.94	.17	0
	2.08	.166	0
	2.8	.172	0
	3.7	.172	0
	6.08	.175	0
	23	.165	0
1,5-Hexadiene	50	NM	3×10^3
	67	NM	1×10^4
	73	.123	2×10^4
	117	.107	1×10^4
	0*	.165	0

* This data point taken during same run as other 1,5-Hexadiene data.

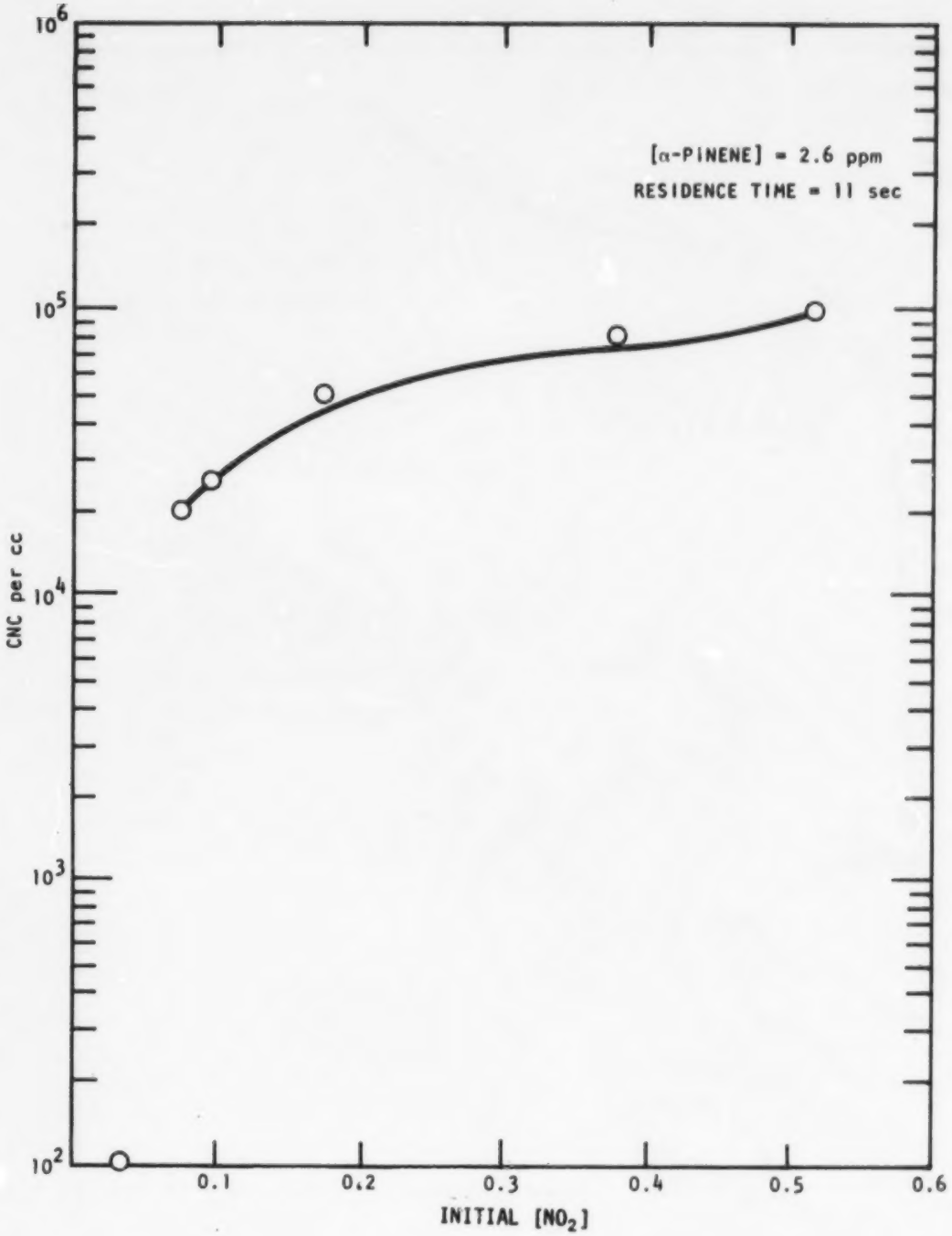

Figure 11. The Effect of Initial NO_2 Concentration on Condensation Nuclei from α-Pinene

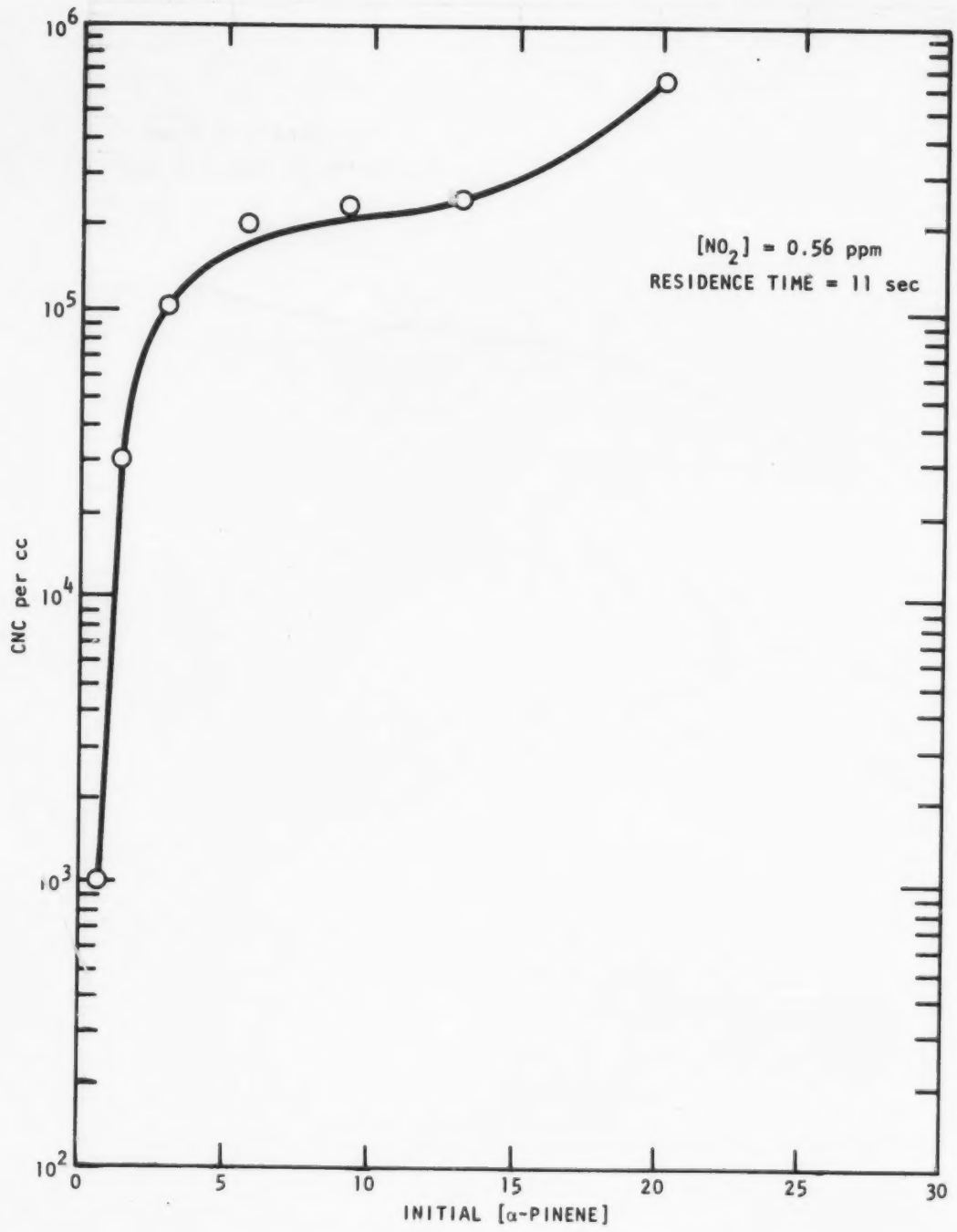

Figure 12. The Effect of Initial α-Pinene Concentration on Condensation Nuclei Production

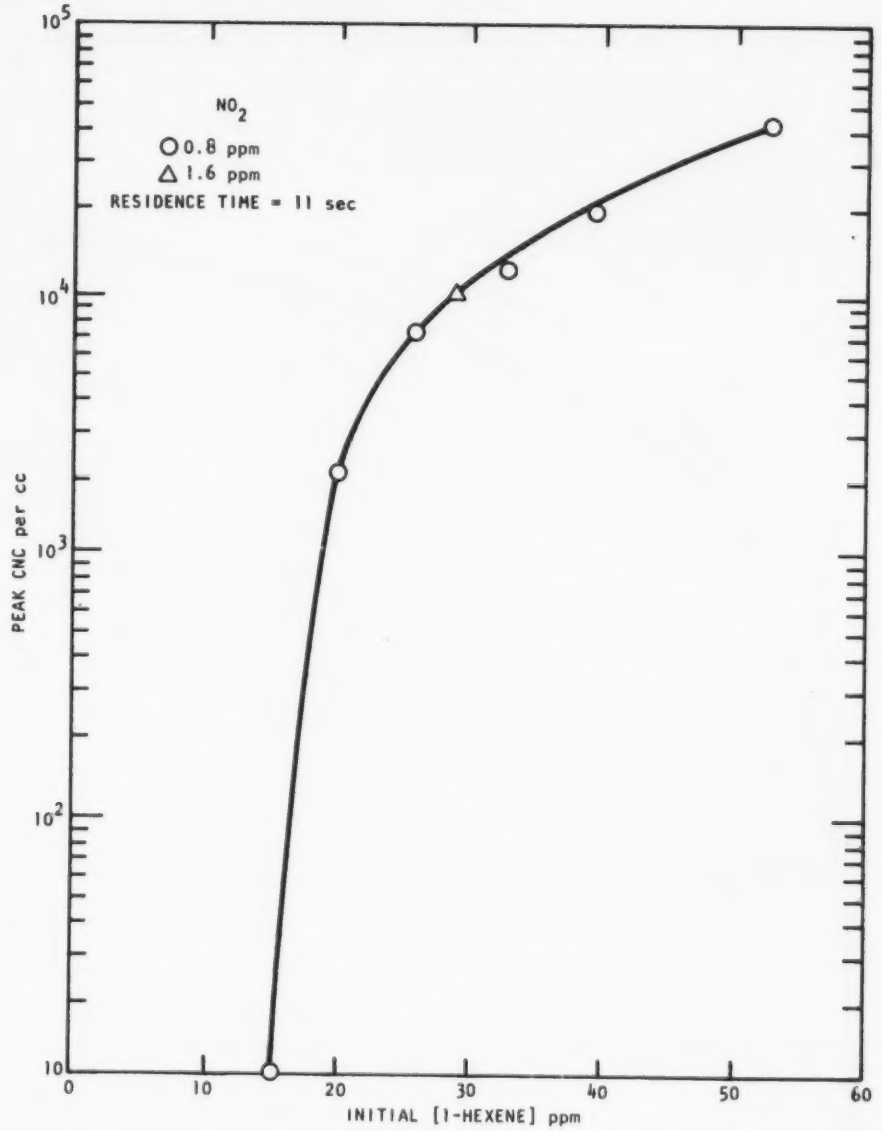

Figure 13. The Effect of Initial 1-Hexene Concentration on Condensation Nuclei. The peak nuclei concentration is plotted since for the case of 1-hexene the disturbance of the probe caused nuclei production to gradually disappear.

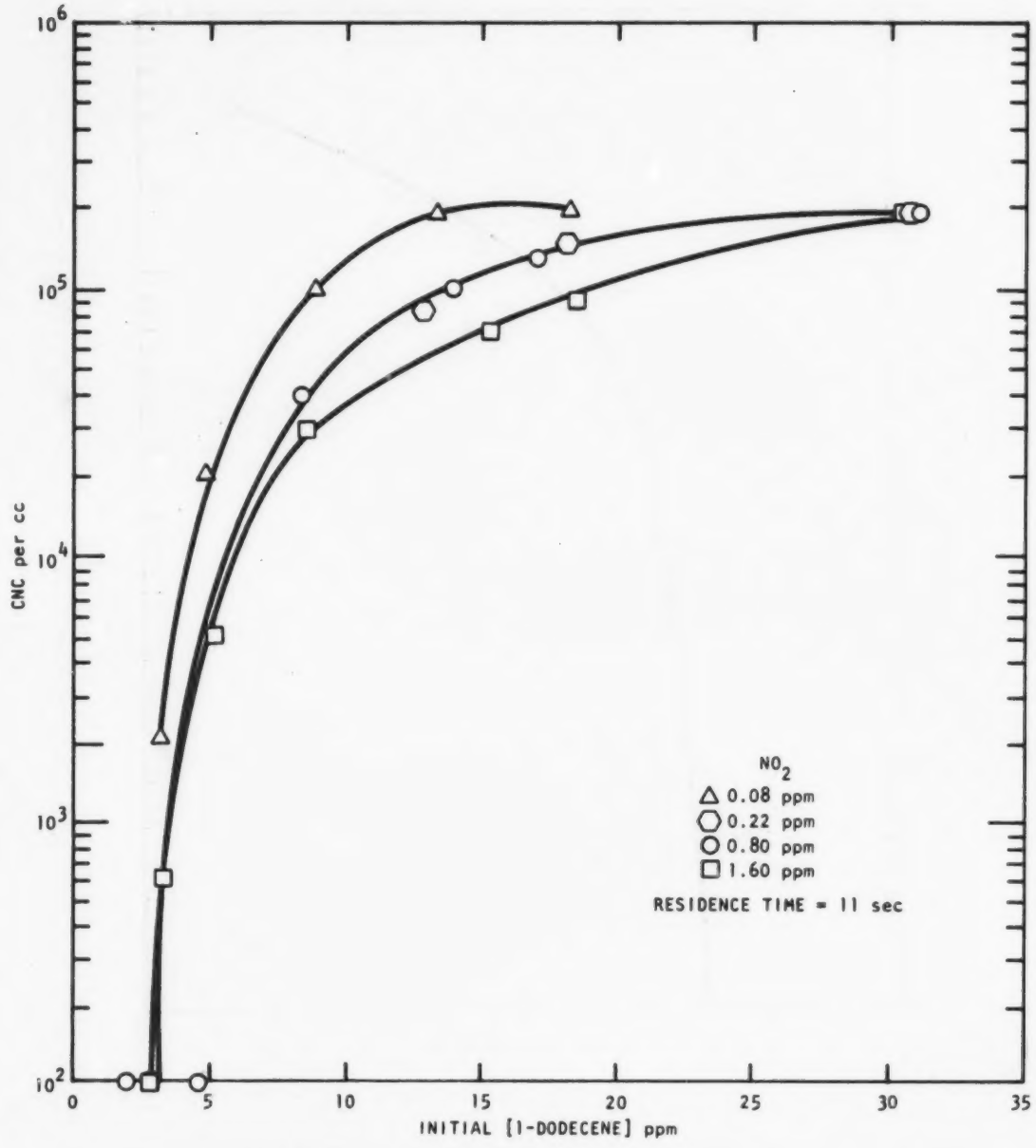

Figure 14. The Effect of Initial 1-Dodecene Concentration on Condensation Nuclei

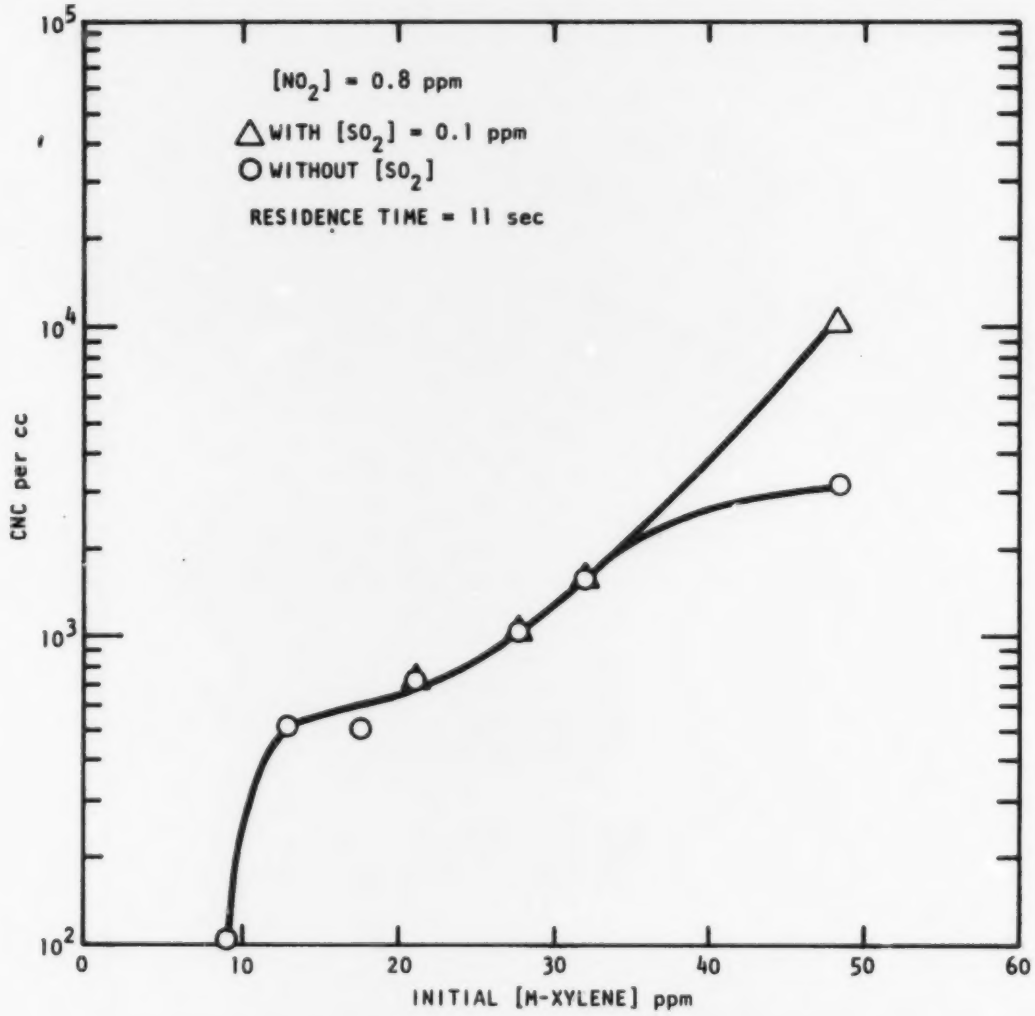

Figure 15. The Effect of Initial M-Xylene Concentration on the Production of Condensation Nuclei Both With and Without SO_2 Present

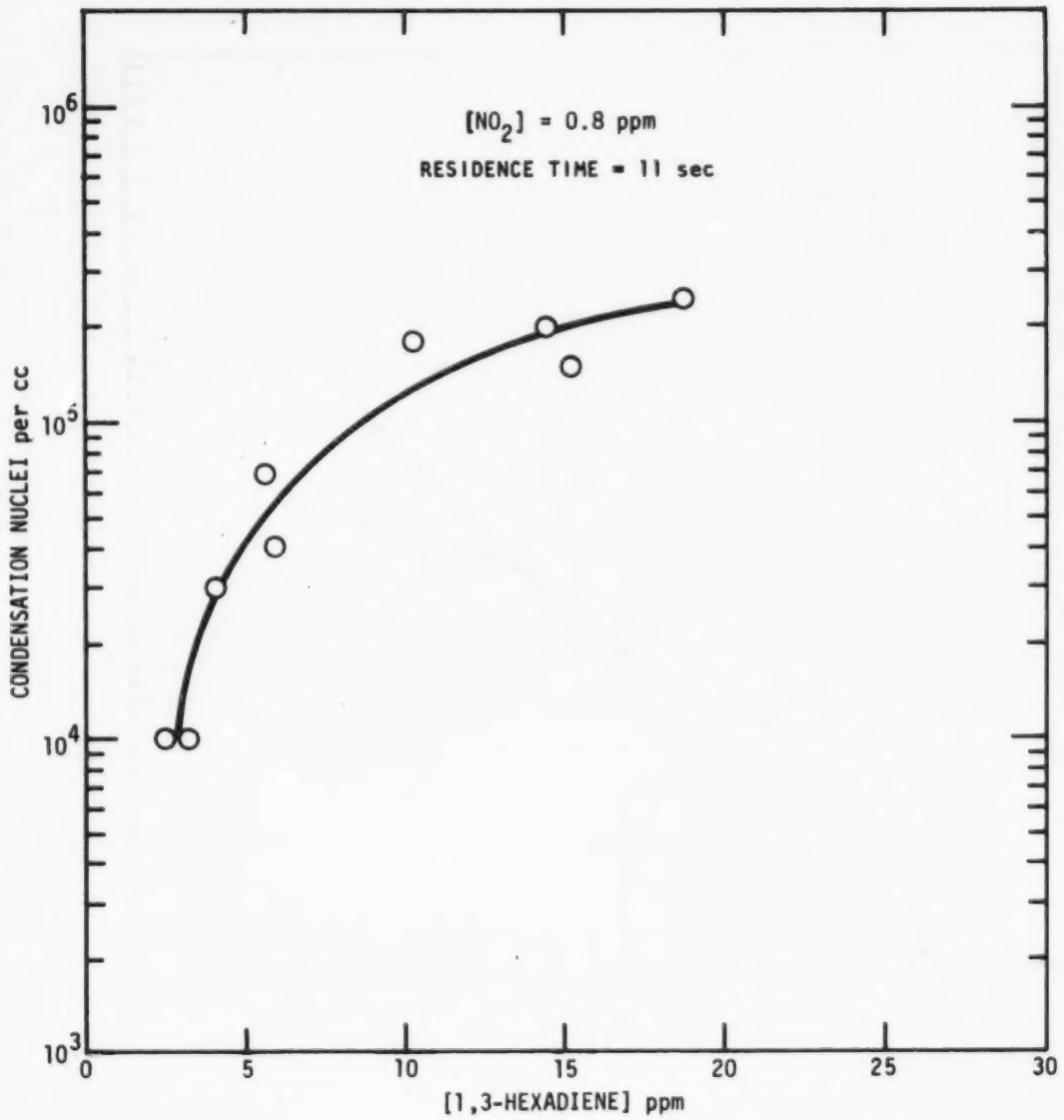

Figure 16. The Effect of Initial 1, 3-Hexadiene Concentration on Condensation Nuclei

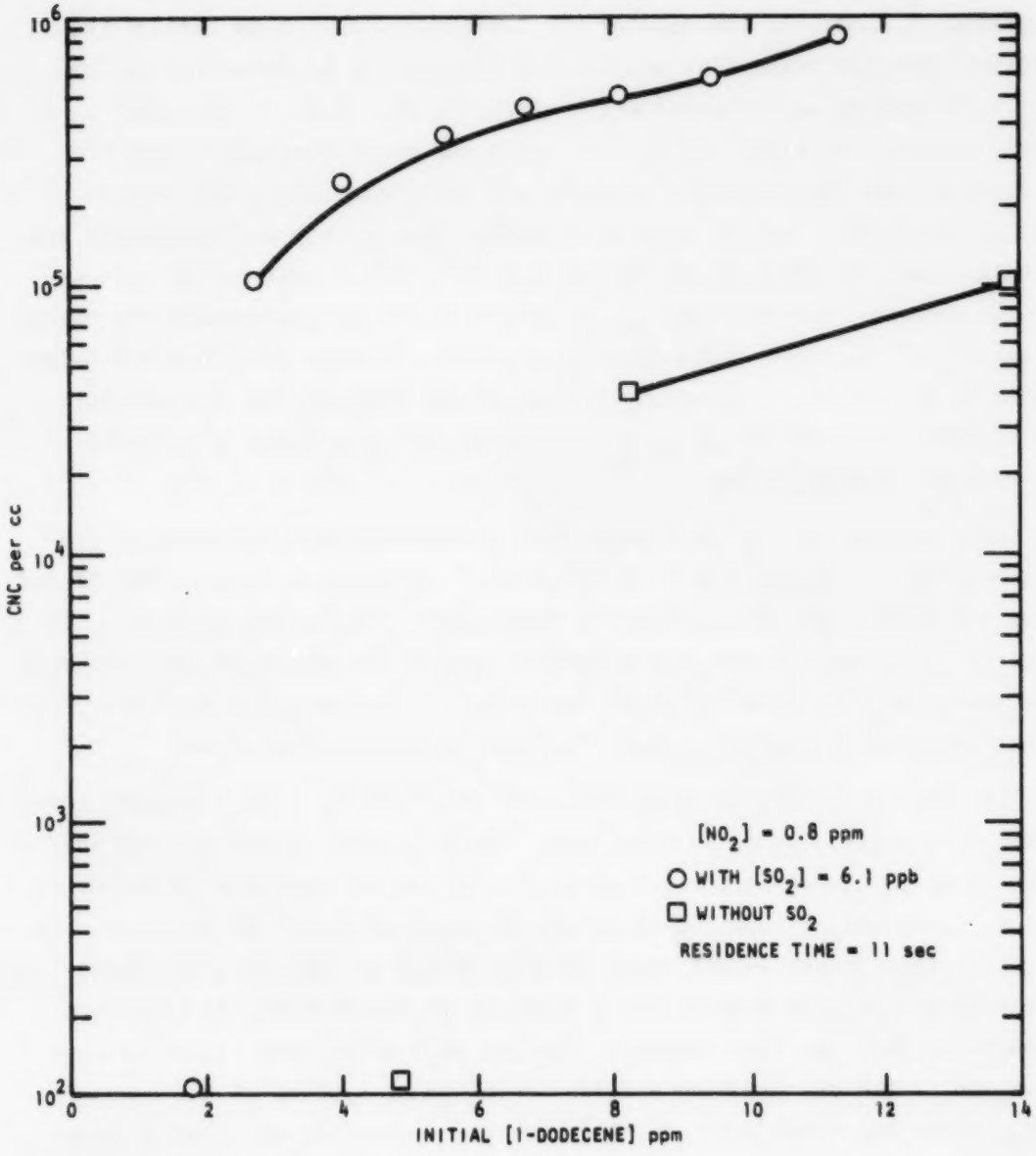

Figure 17. The Production of Condensation Nuclei from 1-Dodecene with SO_2 Present as a Function of 1-Dodecene Concentration

With cyclohexene and 1-hexene, the aerosol production was not stable as a function of time. If the reactor was operated with no flow through the probe and then the probe flow was started through the condensation nuclei counter, a reading was obtained which gradually decreased to zero over a several-minute time span. If at this point the probe flow was turned off and left off and the procedure repeated one half hour later, the aerosol count would return. In the case of 1-hexene, this effect was repeatable and the data shown in Figure 13 represents the peak values obtained in this way. With cyclohexene, the data was not reproducible and no measurement was taken. For several of the other hydrocarbons, a similar behavior was observed below threshold; but once a critical concentration was reached, the measurements were stable. The initial point in Figures 12 and 14 through 17 reflects this critical concentration.

Small amounts of SO_2 were added with three different hydrocarbons present, m-xylene, 1-dodecene and 1,3-hexadiene. As shown in Figures 15, 17 and 18, in all three cases an increase in condensation nuclei was observed. In the cases of 1-dodecene and 1,3-hexadiene, only a few ppb of SO_2 was required to produce almost an order of magnitude effect. However, with m-xylene, 0.1 ppm was required to produce a small increase in nuclei production.

The addition of NH_3 to three different hydrocarbons also increased the condensation nuclei formed in each case. For m-xylene, Figure 21, the increase is only 50%, while for 1-hexene, Figure 19, it reaches a factor of 7, and for 1-dodecene, Figure 20, there was an order of magnitude increase. In each case, this occurs in the range of 3 to 10 ppm of ammonia. One difficulty encountered with ammonia was a decrease in reproducibility after its introduction into the flow reactor. Part of this effect was traced to contamination of the gas handling and flow development systems of the reactor by NH_3. Care was taken with cleaning the system when NH_3 was used in order to assure reproducibility of the data.

The five cases for which water vapor was added are summarized in Table 4. In all these cases water vapor was added at approximately 50% relative humidity and no measurements were made at other water vapor concentrations.

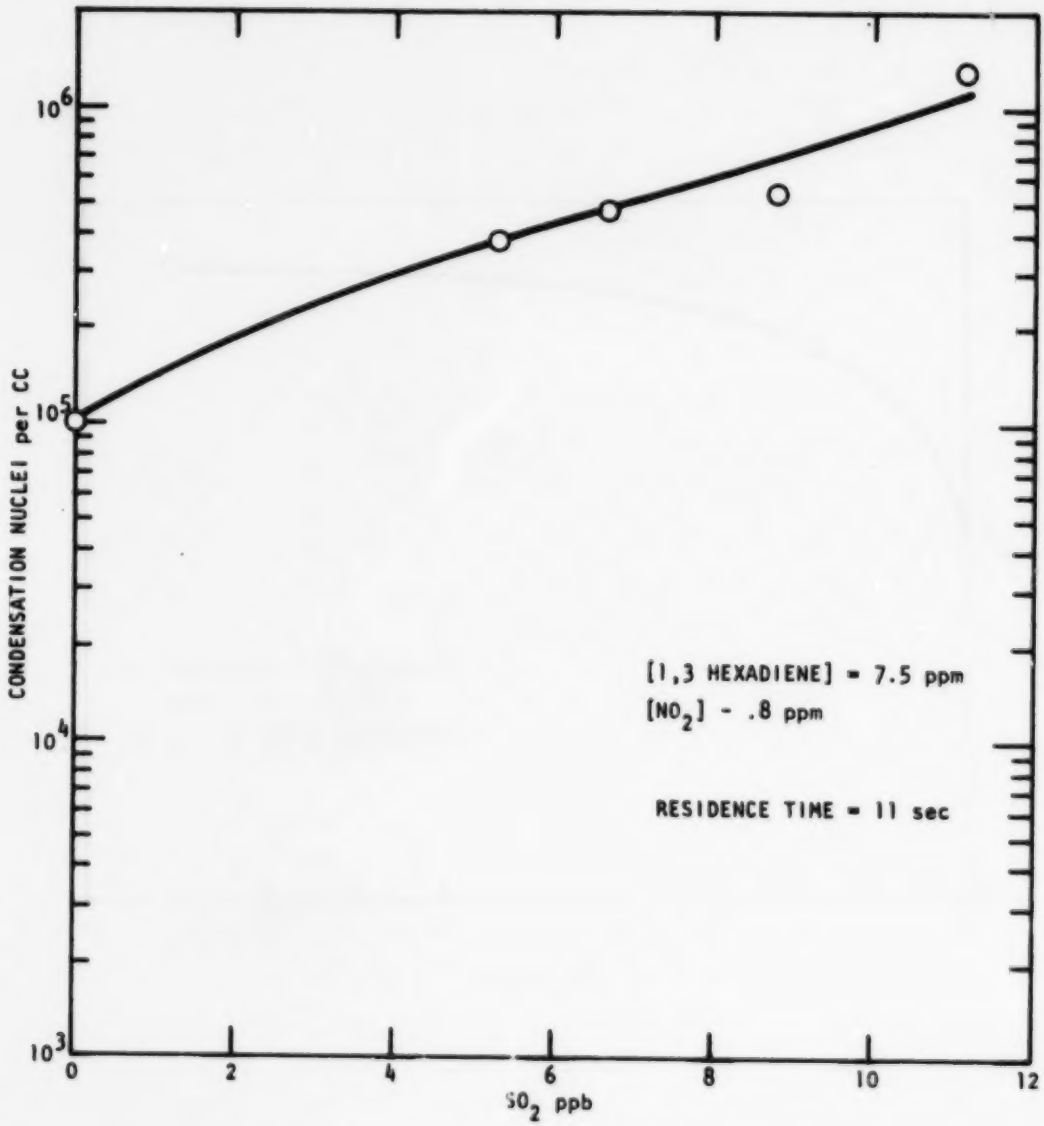

Figure 18. The Effect of SO_2 on Condensation Nuclei Production from 1, 3-Hexadiene

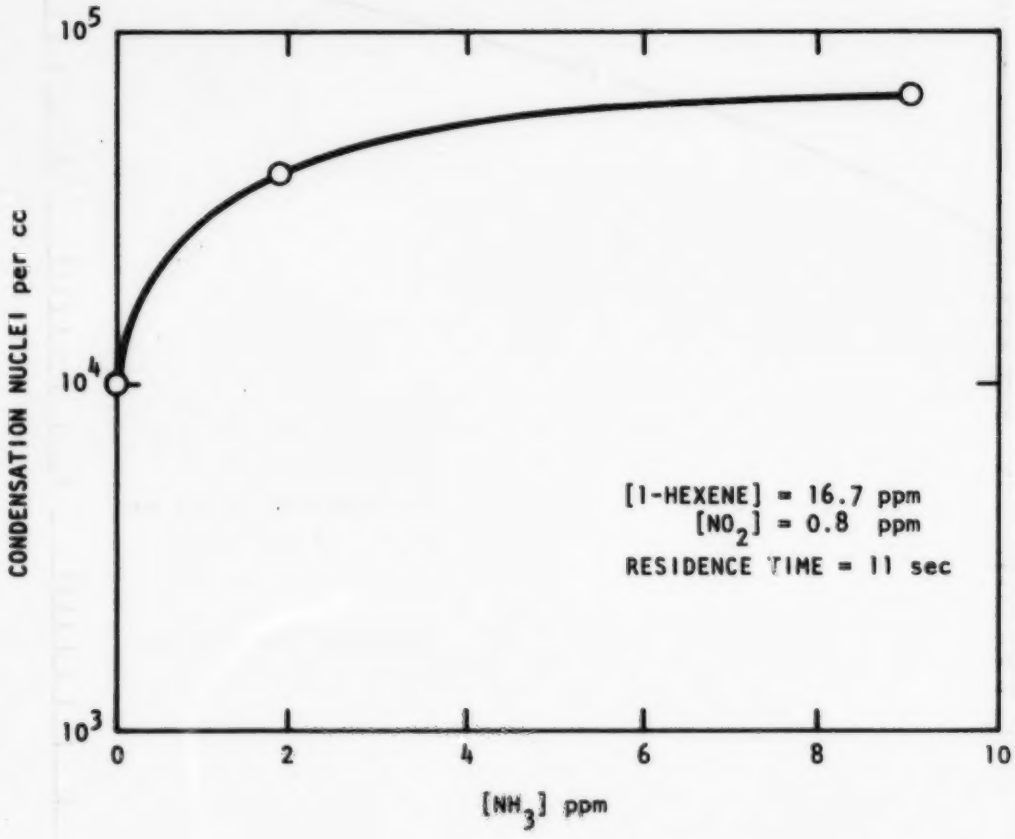

Figure 19. The Effect of NH_3 on Condensation Nuclei Production from 1-Hexene

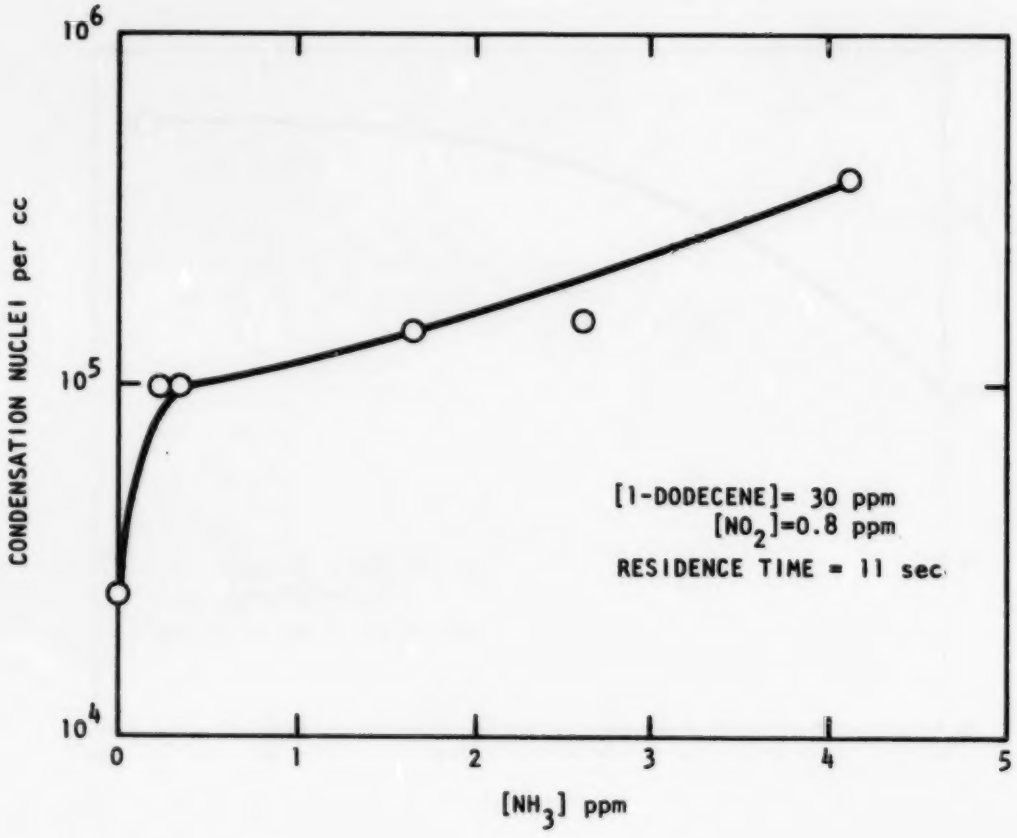

Figure 20. The Effect of NH_3 on Condensation Nuclei Production from 1-Dodecene

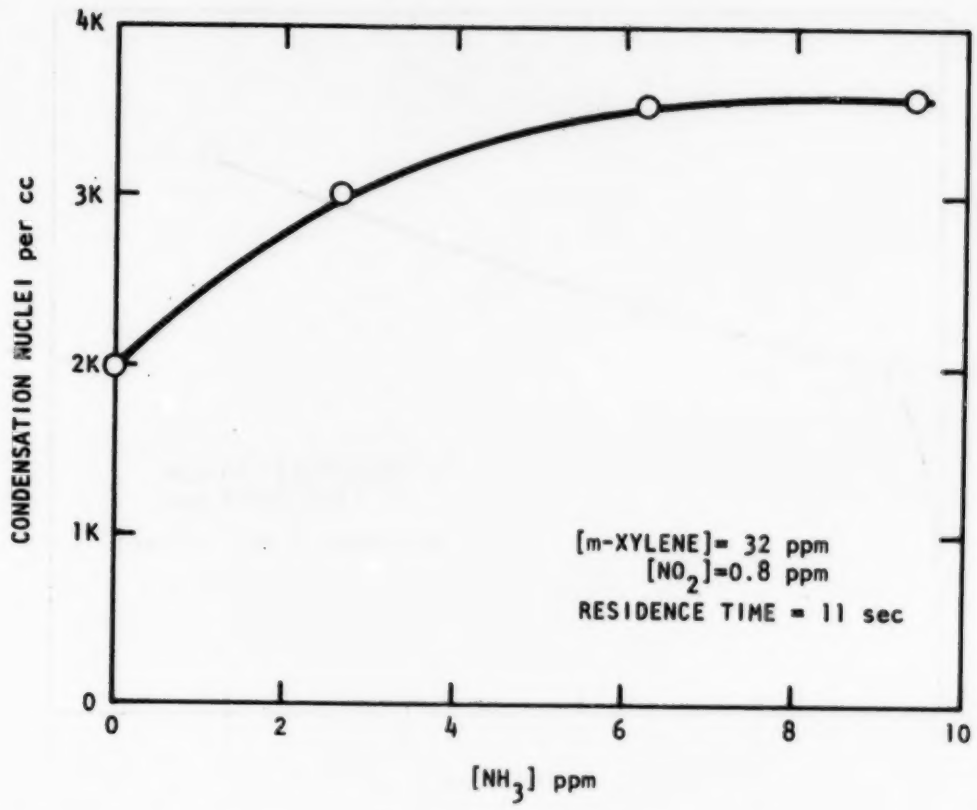

Figure 21. The Effect of NH_3 on Condensation Nuclei Production from M-Xylene

TABLE 4

DATA ON THE EFFECT OF WATER VAPOR AT 50% RELATIVE HUMIDITY

NO_2 Concentration 0.8 ppm

HYDROCARBON	CONCENTRATION OF REACTANTS			PRODUCTS	
	HYDROCARBON (ppm)	NH_3 (ppm)	SO_2 (ppb)	O_3 (ppm)	Nuclei (per cc)
1-DODECENE	32	--	--	0.13	0
	33.5	2	--	0.14	2×10^4
	32	--	4	NM	1×10^4
	43.3	2	6	NM	0
1-HEXENE	18.9	--	--	0.19	0
	18.9	1.3	--	0.19	0

Also only a few single experiments were performed for each case. In all cases the presence of water vapor at 50% relative humidity decreased or eliminated aerosol production. In those cases in which aerosols were present there was an instability in the condensation nuclei number. We consider these data preliminary and plan to pursue this aspect of the problem in more detail in the future.

5.2 Filter Collections

For five of the hydrocarbons and eight cases, filter collections of aerosols were made to determine the actual mass concentration of material produced. These collections are summarized in Table 5. There are several significant facts to be observed in these results. There is not a direct correlation between the number of nuclei formed and the weight gain observed. This is in fact not unexpected due to differences in growth and nucleation rates in the different systems. However, we found a large variation from sample to sample for each hydrocarbon. The largest variation was found with 1-dodecene where the average weight gain was 81.8 μg with an average deviation of 25 μg. All others were much better than this, but there is clear indication that stability over long periods of time must be explored in future work.

Some significant observations are that adding SO_2 to 1-dodecene increased the nuclei count by almost an order of magnitude but did not increase the weight gain. This will be discussed below. Also observed but not understood, with NH_3 and SO_2 present along with 1-dodecene, nuclei counts are extremely high, typically 10^7 per cc, but no material was found on the filters.

5.3 Chemical Analysis

For most of the samples, solvent extraction was performed and an attempt made to take an IR spectrum of the extract. We were successful in three cases in obtaining clear IR spectra. These are presented in Figures 22, 23 and 24.

The spectrum in Figure 22 was obtained from the α-pinene aerosol sample and is shown together with a spectrum obtained by Wilson, Schwartz and Kinzer

TABLE 5

FILTER COLLECTIONS OF AEROSOL SAMPLES

16-hour Collections at 3 l/min

For all cases [NO_2] = 0.8 ppm
Where present [SO_2] = 5.7 ppb
[NH_3] = 2.0 ppm

Hydrocarbon	Hydrocarbon Concentration (ppm)	CNC (per cc)	Weight Gain (μg)	Mass Concentration ($\mu g/m^3$)
1-hexene	50	4×10^4	30	10.4
	50	4×10^4	54	18.8
1-hexene + NH_3	50	5×10^4	45	16.6
	50	5×10^4	65	22.6
1-dodecene	15	10^5	63	21.9
	15	10^5	74	25.7
	15	10^5	91	31.6
	15	1.8×10^5	140	48.6
	15	3×10^5	41	14.2
1-dodecene + SO_2	12	10^6	91	31.6
1-dodecene + SO_2+NH_3	12	10^7	2	-
	12	10^7	0	-
1, 5-hexadiene	70	3×10^4	38	13.2
1, 3-hexadiene	15	2×10^5	55	19.1
	15	2×10^5	53	18.4
α-pinene	20	7×10^5	216	75.0

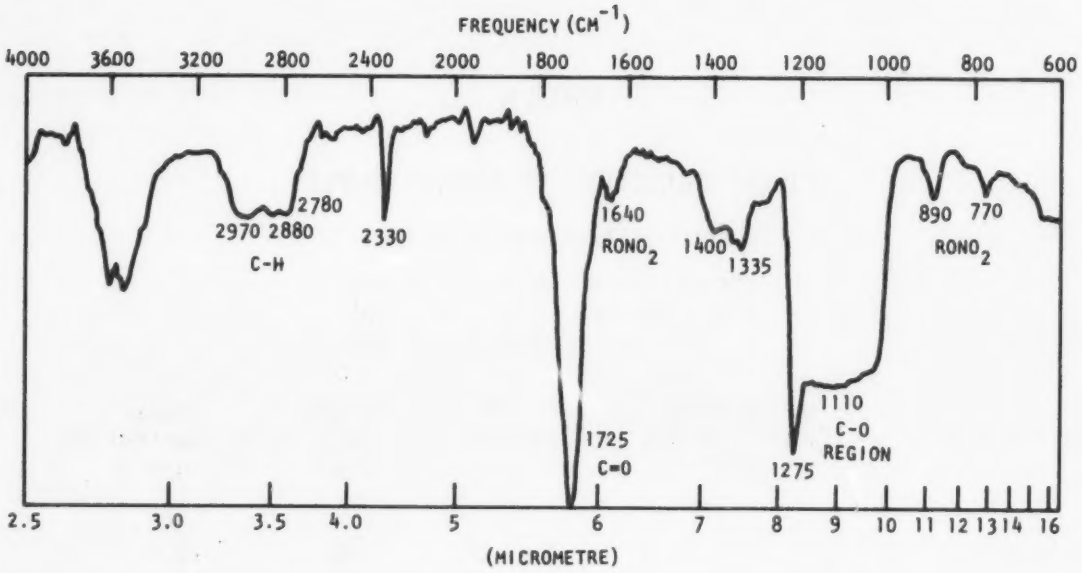

AEROSOL PRODUCED BY IRRADIATING α-PINENE AND NO_2 IN DRY AIR

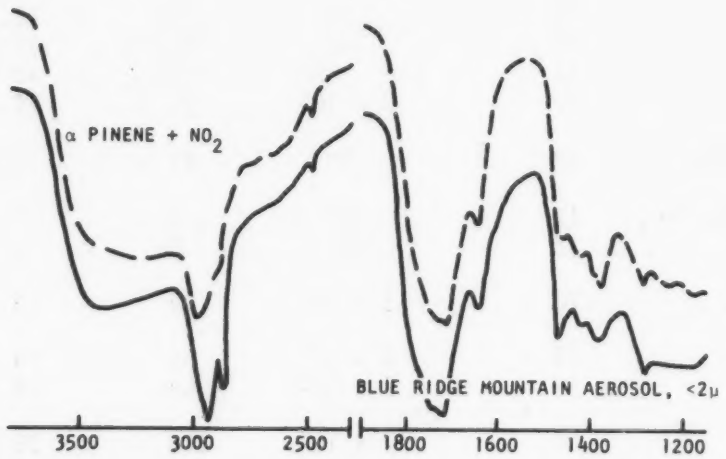

IR SPECTRUM FROM BATTELLE STUDY

Figure 22. Infrared Spectrum of Aerosol Produced by Irradiating α-Pinene and NO_2 in Dry Air. (TOP) Compared with similar results from Wilson, Schwartz and Kinzer at Battelle[2].

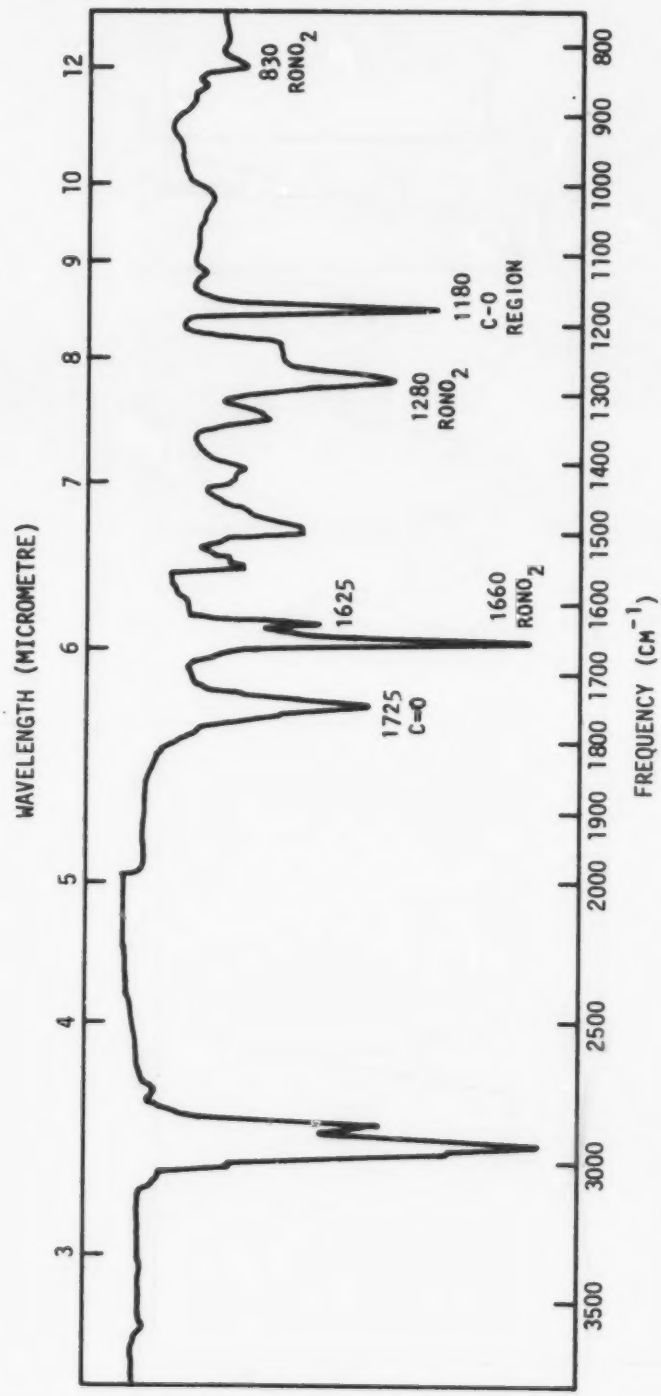

Figure 23. Infrared Spectrum of Aerosol Produced by Irradiating 15 ppm of 1-Dodecene and 0.8 ppm of NO_2 in Dry Air

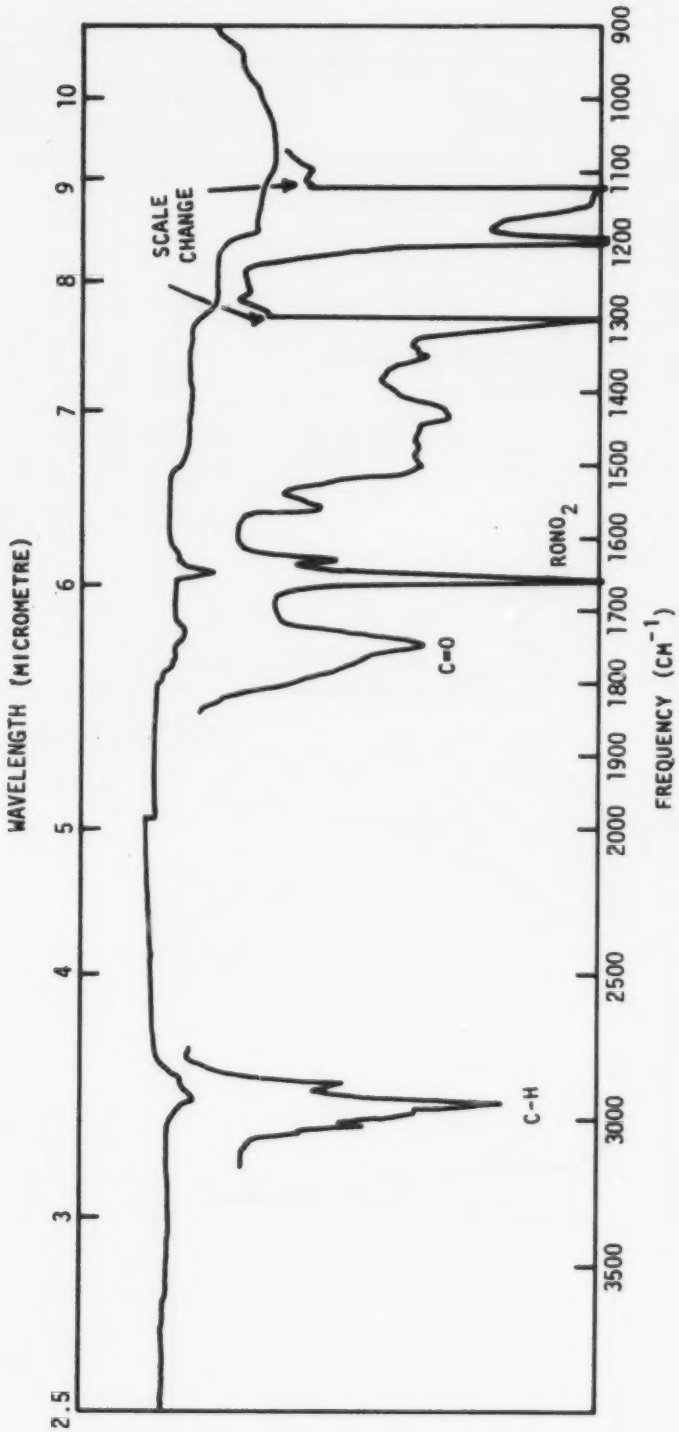

Figure 24. Infrared Spectrum of Aerosol Produced by Irradiating 50 ppm of 1-Hexene, 0.8 ppm of NO_2 and 2 ppm of NH_3 in Dry Air

at Battelle.[2] The general features of these two spectra are strikingly similar. The absorption in our spectrum, near 3600 cm^{-1} is identified as predominately due to contamination by water in the extraction process.

The characteristic C-H absorptions due to stretch around 2900 cm^{-1} are present, although the peak at 2780 is somewhat low. The bending modes at 1400 and 1335 are also present, but the CH_2 scissoring at 1465 cm^{-1}, if present at all, is not clear. The sharpest peak is the carbonyl stretch at 1725 cm^{-1}, which may have a shoulder at 1745 cm^{-1}. Another important feature is the broad peak centered at 1110 cm^{-1}. This is most likely a C-O or O-O type absorption, but it is too broad to be definitely identified. The sharp peak at 2330 cm^{-1} is also present in the Battelle spectrum, but lies in a region with few absorptions. The Battelle group identified the 1640 band as either a C=C or an organic nitrate. If this is in fact the asymmetric stretch of the NO_2 group, then the symmetric stretch, the NO stretch and the NO_2 bending should be found. The symmetric stretch may be on the shoulder of 1335 cm^{-1} peak and the 890 cm^{-1} and 770 cm^{-1} could be the N-O stretch and the NC_2 bending, although both are slightly higher in frequency than would be expected. This nitrate identification must, as a result, be regarded as very tentative.

Figure 23 shows the spectrum obtained with aerosol produced from 1-dodecene. There are some dramatic differences between this spectrum and that from the α-pinene. The C=O band at 1725 cm^{-1} is not as strong even as the C-H stretch bands. The strength of this component, along with the feature at 1280 cm^{-1}, suggests the asymmetric and symmetric nitrate groups, and the single band N-O stretch could be the band at 830 cm^{-1}. This is the most likely analysis of this portion of the spectrum. However, this does not include the 1625 cm^{-1} band which we also see in Figure 24 associated with the 1660 cm^{-1} band. Once again there is a strong absorption in the C-O-C region, but this band at 1180 cm^{-1} is surprisingly sharp.

The spectrum shown in Figure 24 was obtained with aerosol from 1-hexene and NH_3. It is very similar from 1600 cm^{-1} to 3500 cm^{-1} to the 1-dodecene case. The remainder is marked by a very diffuse absorption with some detail

superimposed. It is difficult to say any more about this spectrum than the 1-dodecene case. Both these spectra are marked, however, by a conspicuous absence of an OH absorption. There does not appear to be any group originating from the presence of NH_3; i.e., NH_4^+ or an amino group.

6. DISCUSSION

Ultimately, the goal of this research is to determine how gaseous organic material in the atmosphere becomes part of aerosol material. The emphasis has been on building a technique with which to approach this problem. The important questions to be asked are: what is the material in the aerosols, what are the precursor molecules in the atmosphere, what are the pathways from precursors to aerosols, and what are the kinetics of the process? Each of the aspects of the data and observations of this program is now discussed with these questions kept in mind as well as the general question of the validity of the technique.

One of the most striking aspects of the observations made in this program is the great variation in results from one hydrocarbon to another. This is particularly evident in the ozone production as a function of hydrocarbon concentration. These data are not directly aerosol measurements; however, we will argue below that there is a connection between ozone and aerosol production.

6.1 Hydrocarbon Effect on Ozone Production

In Figure 25 we have brought together all of the data on ozone production, as a function of hydrocarbon concentration for six different hydrocarbons, which was already presented singly in Figures 5-10. We immediately see that photolysis of the initial NO_2 cannot account for all of the ozone production since in several cases the ozone concentration increases with increasing hydrocarbon concentration. Thus in eleven seconds of residence time sufficient photochemistry is taking place to dramatically increase ozone production in some cases. It is also clear that as hydrocarbon concentration increases the ultimate result is a decrease in ozone production for the majority of cases studied.

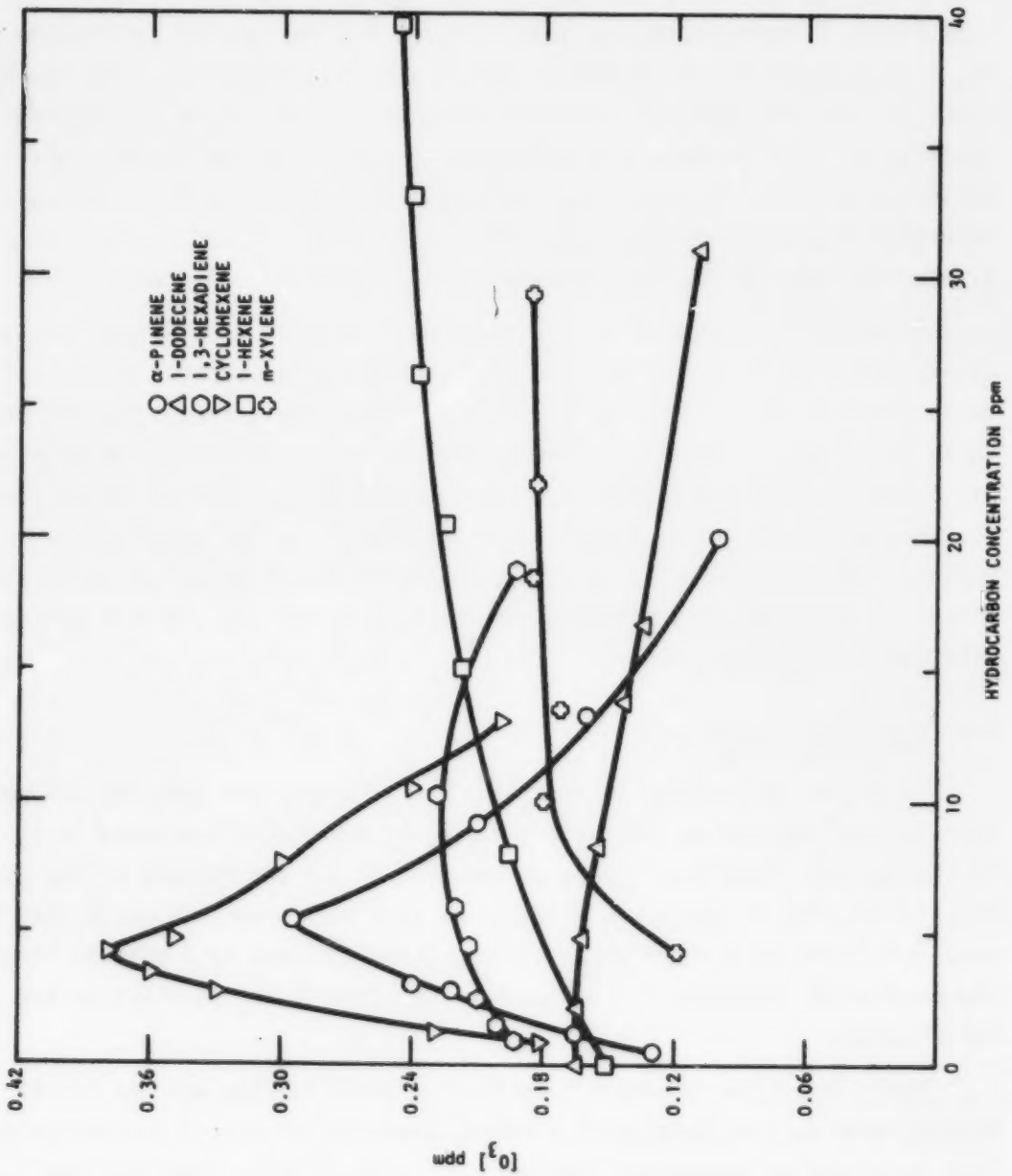

Figure 25. Ozone Production as a Function of Hydrocarbon Concentration for Various Hydrocarbons Irradiated in Dry Air Containing 0.8 ppm NO_2.

It is probable that the ozone production is related to hydrocarbon reactivity, but we do not yet have enough cases to test such a correlation. From Figure 7, however, we see that at least for the case of cyclohexene the NO_2 concentration has an important effect on ozone production. For low NO_2 there is less photochemical activity and thus less effect on ozone production. The high NO_2 case is more difficult to understand than the low NO_2 case. Certainly at almost 3 ppm of NO_2 the reaction of ozone and NO_2 is becoming important but it is not clear why there is no effect of hydrocarbon since at the intermediate NO_2 concentrations cyclohexene has the greatest effect.

Returning to Figure 25 in the three cases where a drop occurs, we have attempted to fit the drop in ozone with increasing hydrocarbon concentration to a simple first order mechanism. The result is that, except for the last three points in the case of α-pinene, the drop in ozone production does not fit a simple first order removal. The complete explanation of these effects requires more data and more analysis. The one conclusion which can be reached, that photochemical reactions involving the hydrocarbons are taking place, is important in justifying the validity of the flow reactor concept with short residence times.

6.2 Nuclei Production

In Figure 26 we bring together the nuclei production data for all runs with just a hydrocarbon, NO_2, and dry air, as previously presented in Figures 12 through 16. From this figure we immediately see the pattern of the data, which except for m-xylene, is a family of parallel curves all exhibiting the same rapid rise with hydrocarbon concentration followed by a plateau region. The pattern for m-xylene is similar but its curve is not parallel to the other curves.

It is necessary to make a quantitative model to know whether one is dealing with self-nucleation of a single component or binary nucleation or some more complex phenomena. However, it is possible to show that the condensation nuclei production data is qualitatively consistent with a simple model. If we assume that we are dealing with the self-nucleation

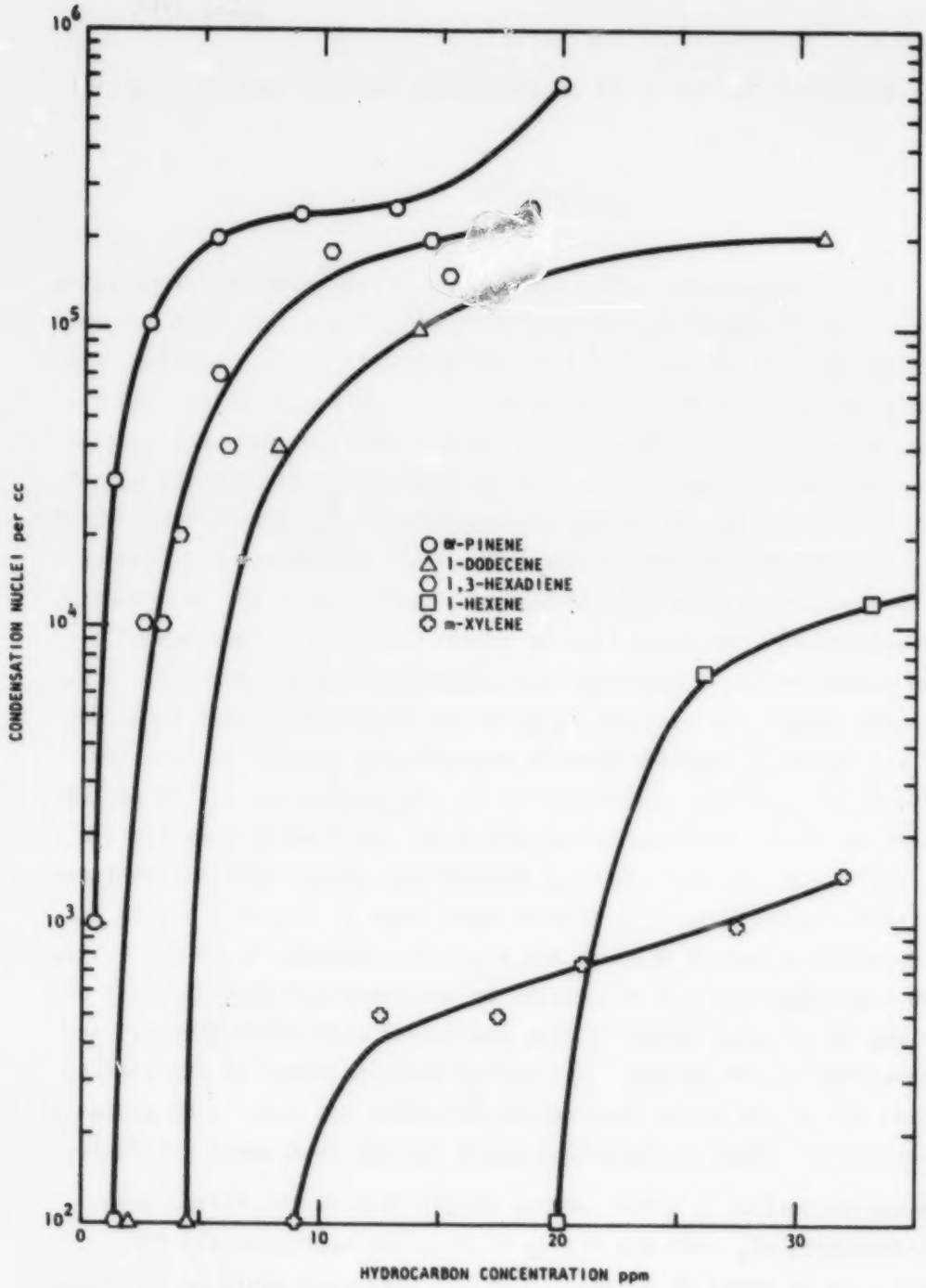

Figure 26. Condensation Nuclei Production as a Function of Hydrocarbon Concentration for Various Hydrocarbons Irradiated in Dry Air Containing 0.8 ppm NO_2.

of a single component, we may write an expression for the rate of formation of nuclei[9]

$$J = AS^2 e^{-B/\ell n^2 S}$$

where S is the supersaturation ratio for the nucleating component (the ratio of the actual vapor pressure to the equilibrium vapor pressure) and A is a function of the density of the liquid in the drop, its surface tension, its equilibrium vapor pressure for a flat surface, its molecular weight and the temperature, while B is a function of the surface tension, the density, the molecular weight and the temperature. If we further assume that the nuclei concentration is linear in the production rate and the supersaturation ratio is linearly proportional to the initial hydrocarbon concentration, then we may use this equation to make qualitative predictions about the condensation nuclei concentration. The rapid rise in nuclei number as a function of hydrocarbon concentration occurs when the exponential term dominates. However, as S gets larger the rate of change of the exponential term shows and eventually the nuclei production rate is dominated by the AS^2 factor. Unfortunately, A, B, and S are determined in part by properties of the nucleating substance which in this case is unidentified, which makes quantitative comparison difficult. We feel that the form of our nuclei data is consistent with homogeneous nucleation. The form of data shown in Figure 3 may be fitted by selected values of A and B and a relation between S and the initial hydrocarbon concentrations but it remains to be determined whether a set of parameters may be selected which is also consistent with other physical and chemical knowledge of the system. We suspect that the onset of the plateau is too rapid, but in the short time period this does not seem to be accounted for by coagulation. Other explanations could include instrument artifacts.

As we saw in Section 5.3 the average weight gain of the filter when sampling 1-dodecene, NO_2, and dry air is 81.8 μg for approximately 10^5 particles/cc. In 16 hours at 3 l/min. 2.9×10^{11} particles would be collected and for 81.8 μg this is 2.8×10^{-16} grams per particle. Assuming the density of the condensed material of 1 gm/cc we find a particle average radius of

0.04 micrometre. This is a reasonable value in comparison to atmospheric size ranges. It is also interesting that the addition of SO_2, for the case of 1-dodecene, produced a dramatic increase in the condensation nuclei, but as we see from the data of Table 3, there is no proportional increase in weight gain. What is probably happening here is that in the presence of SO_2 a new condensable material is produced which has a smaller critical nucleus and hence a higher rate of nuclei production. The bulk of the material could remain similar to that obtained without SO_2; further data are required to establish this.

Another effect which must be explained is that of instabilities in aerosol production in the bases of 1-hexene and cyclohexene. We feel that this is related to the stirring effect observed by W. E. Wilson at Battelle.[10] The most important part of his observation is that once formed, aerosols are not appreciably removed by stirring; but their formation is quenched by stirring. The sampling probe was not operating isokinetically during measurements of condensation nuclei, so some flow shear was present at the probe inlet. If this instability is sufficient to quench aerosol production (as the stirring does) and if the nuclei are not formed until they reach the vicinity of the probe, their formation will be quenched by the operation of the probe. Furthermore, the time scale for the onset of the quenching will not be determined by the average flow but rather by the rate at which the flow instability grows after the initial disturbance. These time constants were found to be large in the flow visualization measurements. If, on the other hand, the aerosols are produced before the flow disturbed region, they are probably not affected significantly by the flow disturbed region.

6.3 Speculations About Mechanism

A very promising aspect of the present work is the ability to collect and analyze samples. The three IR spectra presented here are only a preliminary view of what can eventually be done. The most significant aspect of our spectra is that there is no strong acid component identified (in the α-pinene case, this interpretation is not as certain); however C=O is

definitely present, and some C-O linkage as well as an organic nitrate is consistent with the results. The only limit on mechanistic models to fit such simple facts is one's imagination; however, starting from a recent proposed gas phase, ozone-olefin reaction mechanism of O'Neal and Blumstein,[11] one can construct a plausible hypothesis. They suggest that after the initial attack on the double bond by ozone, the molozonide formed, instead of undergoing a Criegie split, becomes a biradical:

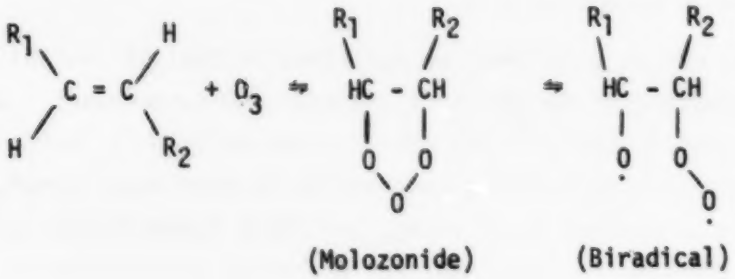

(Molozonide) (Biradical)

One possible path at this point that O'Neal and Blumstein suggest is the abstraction of a hydrogen by the two oxygen chain from the carbon with one oxygen (α-hydrogen abstraction). One possible result of this is:

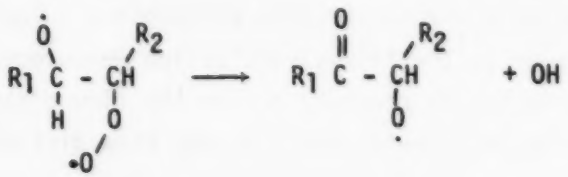

Radicals such as these when terminated by an NO_2 would produce the features we see in the IR spectra. A few steps of polymerization with the olefin present are also possible, leading to heavier, more condensable species. Another possible product from such a rough mechanism is a peroxyacylnitrate which also has all the required functional groups.

6.4 Atmospheric Aerosol Processes

The fact that a mechanism can be constructed to fit the IR data which involves ozone raises the possibility that ozone is a key in forming aerosols with olefins present. This has been discussed before, for example by Groblicki and Nebel.[3] By juxtaposing some of our condensation nuclei data with atmospheric data we can get some further evidence for the importance of ozone-olefin reactions in aerosol production. If the data of Figures 4 and 11 is replotted to eliminate $[NO_2]$ as a variable, we obtain in Figure 27 a strong correlation between condensation nuclei and ozone concentration for a fixed hydrocarbon concentration. Although α-pinene is not a typical urban hydrocarbon it was the only one for which we had sufficient data to make the comparison. Figure 28 shows the correlation between peak ozone and b_{scat} (the extinction coefficient for scattering of light by aerosols) from the California Aerosol Characterization Experiment for the summers of 1972 and 1973.[1] We feel that these correlations are not coincidental and that, in particular, our data is pointing to a strong contribution of ozone-olefin reactions to aerosol production in urban atmospheres.

The conditions in the atmosphere are much more complex than those in our reactor. In particular there are many more gas phase components present and there are both natural and anthropogenic primary aerosols. As far as complexity of the gas phase is concerned we have done no experiments which test the synergistic effects of multiple hydrocarbons present at once; however we have made preliminary experiments with trace inorganic components. We have found that water vapor at 50% relative humidity has a strong quenching effect on aerosol production from olefins (the only cases tried) although it does not affect the ozone production in these cases. Ammonia at 10 ppm made a significant increase in condensation nuclei and SO_2 at concentrations as low as 6 ppb produced a dramatic increase in condensation nuclei.

In order to relate our condensation nuclei production results to the atmosphere one must realize that we only see results of homogeneous nucleation. These products if they nucleate homogeneously will condense even more readily on already existing nuclei in the atmosphere. Thus any material we

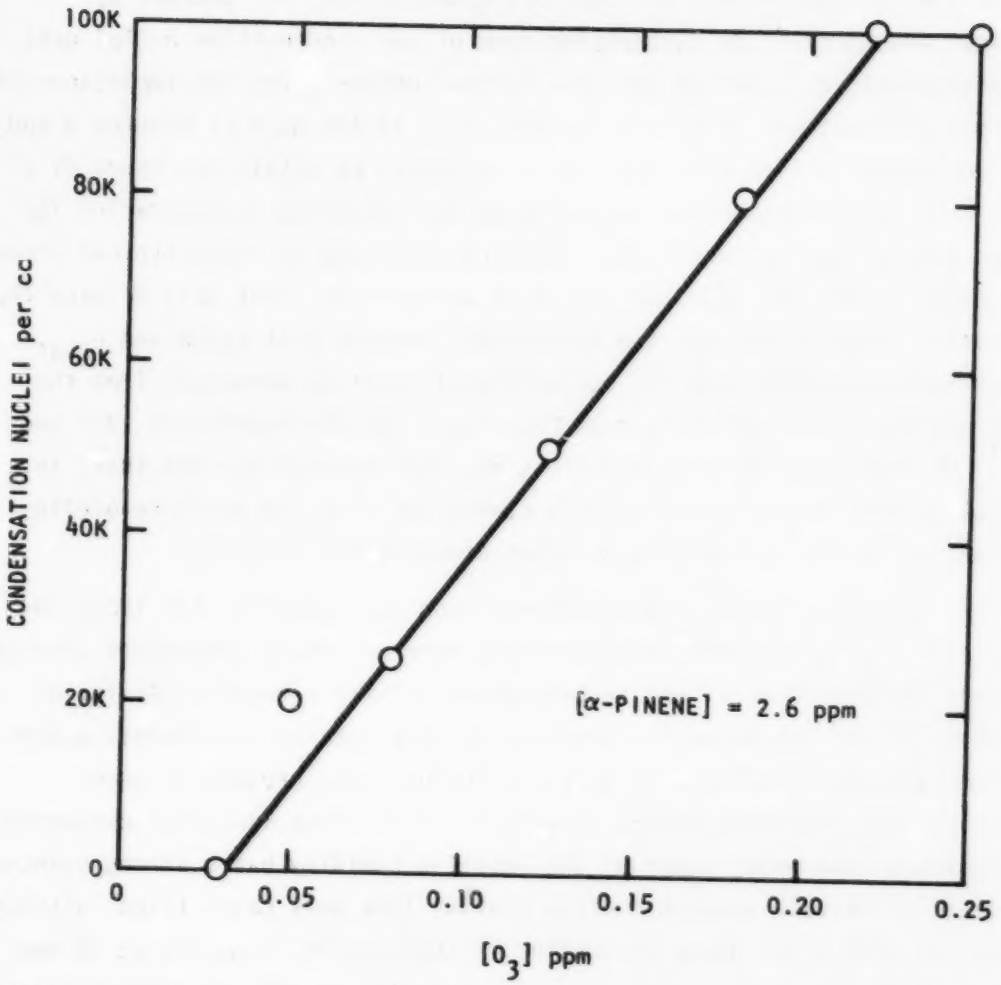

Figure 27. Dependence of Condensation Nuclei on O_3 Concentration with Fixed α-Pinene. This Data is from Figures 4 and 11

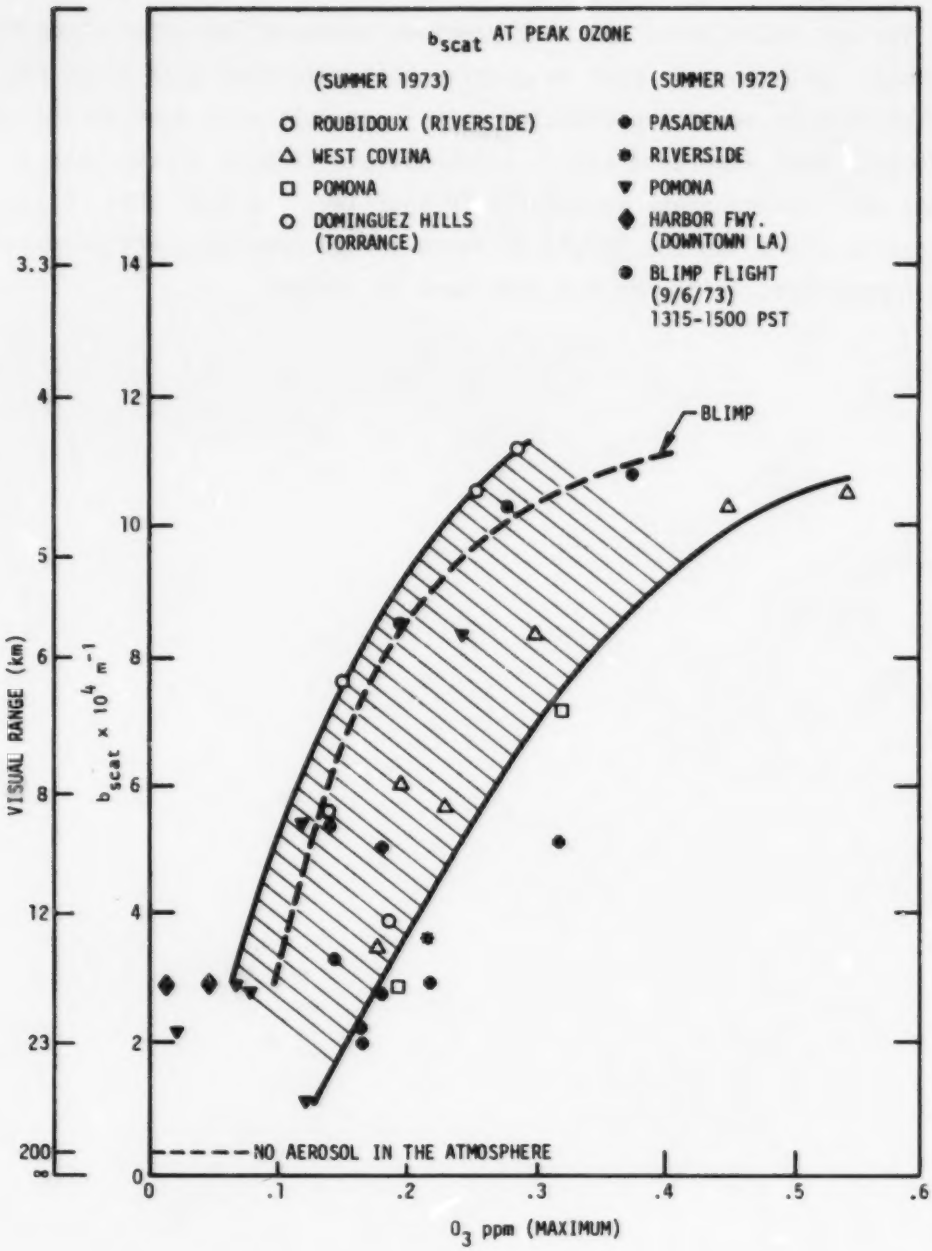

Figure 28. Dependence of Light Scattering Aerosol upon Peak Ozone Concentration as observed at Various Places in California During the California Aerosol Characterization Experiment.

see is to be definitely expected in the atmosphere, while the absence of an effect for our experiments does not preclude condensation under atmospheric conditions. With this in mind we observe that molecular size plays an important role in aerosol production with large molecules more active, but structure is very important also. 1,3-hexadiene is more active than 1-dodecene and 1,5-hexadiene is relatively inactive. We feel that it is important to establish the levels of larger, more complex olefinic molecules in the atmosphere, which has not been done at present.

APPENDIX A - Theory of A Dilution Probe

Some measurements presented in Section 2.1 of this report were made with the use of a dilution probe. The design of this probe has been previously presented.[5] Its use is shown in Figure 1. This appendix contains theoretical explanation of the effects observed.

We shall assume that there are two chemical species of interest: X is the concentration of the component we intend to measure, and Y is the concentration of the component which reacts with X following a simple second order rate law,

$$\frac{dx}{dt} = -kXY \quad .$$

We will further assume that X_0 and Y_0 are the concentrations of the two components at the entrance to the probe. We define two further parameters γ and β such that $Y_0 = \gamma X_0$, and βX_0 is the concentration of species to be measured after dilution. The assumption is made that the dilution is instantaneous and therefore β varies from 1 to 0 as the dilution flow increases, since the total flow through the probe is held constant.

We may now examine the data from Figure 1 and make an initial observation. Let us assume that $\gamma = 0$ and $\beta = 1$ so that we have no dilution and no dark reactions in the probe. The measurement after flow through the probe gives X_0 directly. (In this case X_0 is the concentration of ozone). If β now varies the measured concentration X will be given by βX_0, a linear relationship. For all data in Figure 1 this function is called the "apparent theoretical dilution curve." It is the only function that can be determined from just X at $\beta = 1$ and the total probe flow which determines the scale of β. As long as $\gamma = 0$ the measurements follow the "apparent theoretical dilution curve." If γ is not zero then k and t, the time in the probe, must be known to calculate the true dilution curve.

In order to calculate the true dilution curve we must solve a pair of simultaneous differential equations,

$$\frac{dx}{dt} = -kXY$$

$$\frac{dy}{dt} = -kXY$$

with $X(t=0) = \beta X_0$ and $Y(t=0) = \gamma\beta X_0$.

The solution of these equations yields,

$$\frac{X}{X_0} = \frac{(\gamma-1)e^{-(\gamma-1)\beta X_0 kt}}{\gamma - e^{-(\gamma-1)\beta X_0 kt}}$$

In Table A and Figure 29, for one set of values of the parameters, the true and apparent dilution curves are shown. We see at once that the concentrations along the true dilution curve are greater than those along the apparent dilution curve. This can be shown to be true in general and it is possible for X to increase for decreasing β, so that dilution causes the observed concentration to increase. This can be understood intuitively if we observed that dilution affects both X and Y and thus the rate of removal of X is proportional to β^2 while the decrease in X due to dilution is proportional to β. Since β is always less than 1, increasing dilution flow and thereby decreasing β will reduce the affect of reactions faster than it will decrease the concentration by dilution.

TABLE A

Comparison of True and Apparent Dilution Curves

$\gamma = 1.5$, $kT = 1$ and $X_0 = 1$

β	X	Apparent Dilution Curve
1	0.34	0.34
0.9	0.33	0.306
0.8	0.32	0.272
0.7	0.31	0.238
0.6	0.29	0.204
0.5	0.27	0.17
0.4	0.24	0.136
0.3	0.20	0.102
0.2	0.15	0.068
0.1	0.87	0.034
0.05	0.046	0.017
0.01	0.0099	0.0034
0	0	0

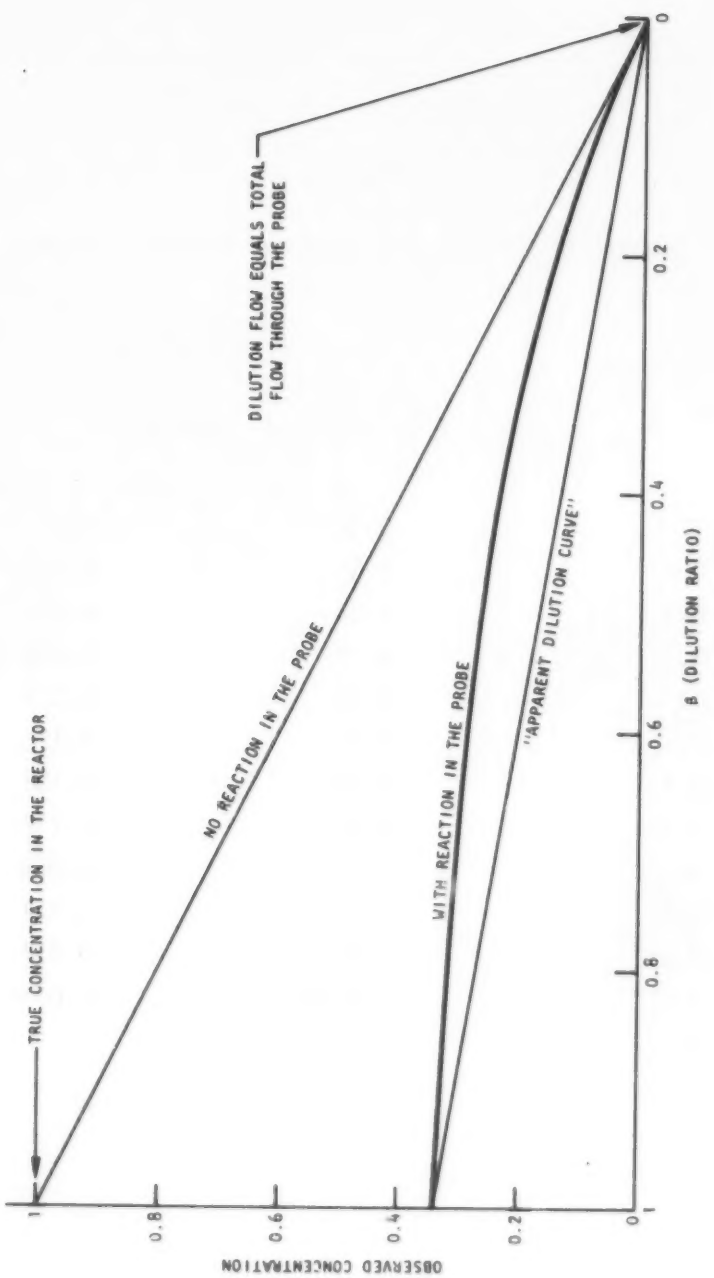

Figure 29. Comparison of True and Apparent Dilution Curves.

APPENDIX B - Conditions for a Typical Experimental Run

In this appendix we tabulate the conditions and values of parameters set and measured for a one typical run. Entries marked with * are calculated from the others.

1. Flow Rates

Dry Nitrogen	- 7.80 ℓ/min
Dry Oxygen	- 1.78 ℓ/min
Nitrogen saturated with 1-Dodecene	- 200 cc/min
Nitrogen containing 183 ppm NO_2	- 41 cc/min
*Total Flow	- 9.82 ℓ/min
*Residence Time	10.8 sec
Probe Flow when measuring Ozone	1 ℓ/min
Probe Flow when measuring Nuclei	2.1 ℓ/min
No Dilution Flow used for any Runs	

2. Concentrations

Nitrogen	79.4%
Oxygen	18.1%
NO_2	0.76 ppm
1-Dodecene	17 ppm

3. Other Parameters

Cooling Water Temperature	23°
*Gas Temperature (Determined by Cooling Water)	23°
Irradiation	
Three lamps on	
No Filter solutions	

LAMP SPECTRUM (Ref.5)

Mercury Lines (nanometre)	Radiated Energy watts
546.1	34.0
435.8	29.0
404.5	15.9
366.0	40.5
334.1	3.8
313.0	21.0
302.5	11.3
296.7	6.5
289.4	2.3

4. Results

Ozone Concentration	0.135 ± .009 ppm
Condensation Nuclei Concentration	135K ± 15K per cc

REFERENCES

1. G. M. Hidy et al., "Characterization of Aerosols in California" Report SC524.25FR, Science Center, Rockwell International, Thousand Oaks, Calif. (1974).

2. W. E. Wilson, W. E. Schwartz and G. W. Kinzer, "Haze Formation--Its Nature and Origin," Final Report EPA-CPA70-Neg. 172, Jan. 1972.

3. P. J. Groblicki and G. J. Nebel in "Chemical Reactions in Urban Atmospheres," Ed. C. S. Tuesday, Amer. Elsevier, N.Y. 1971.

4. W. C. Kocmond et al., "Determination of the Formation Mechanisms and Composition of Photochemical Aerosols," Calspan Report No. NA5365-M-1 prepared for EPA contract 68-02-0557 and CRC-CAPA-8-71. Calspan Corp., Buffalo, N.Y.

5. M. Lipeles et al., "Mechanism of Formation and Composition of Photo-Chemical Aerosols," Final Report EPA-R3-73-036, July 1973.

6. P. A. Leighton, "Photochemistry of Air Pollution," Academic Press, N.Y. 1961.

7. G. H. A. Cole, "Fluid Dynamics," Wiley, N.Y. 1962, p. 119.

8. Ibid, p. 130.

9. H. R. Byers, "Elements of Cloud Physics," University of Chicago Press, Chicago, IL 1965, p. 46.

10. W. E. Wilson, Jr. - Discussion section after Ref. 3.

11. H. E. O'Neal and C. Blumstein, Int. J. Chem. Kinetics V, 397 (1973).